NOAA Technical Memorandum ERL WPL-66

THE FORMATION OF ELEVATED REFRACTIVE LAYERS IN THE OCEANIC BOUNDARY LAYER BY OFFSHORE MODIFICATION OF LAND AIR

Earl E. Gossard

Wave Propagation Laboratory
Boulder, Colorado
December 1980

noaa NATIONAL OCEANIC AND ATMOSPHERIC ADMINISTRATION / Environmental Research Laboratories

NOAA Technical Memorandum ERL WPL-66

THE FORMATION OF ELEVATED REFRACTIVE LAYERS IN THE OCEANIC BOUNDARY LAYER BY OFFSHORE MODIFICATION OF LAND AIR

Earl E. Gossard

Wave Propagation Laboratory
Boulder, Colorado
December 1980

UNITED STATES
DEPARTMENT OF COMMERCE
Philip M. Klutznick, Secretary

NATIONAL OCEANIC AND
ATMOSPHERIC ADMINISTRATION
Richard A. Frank, Administrator

CONTENTS

THE FORMATION OF ELEVATED REFRACTIVE LAYERS IN THE OCEANIC BOUNDARY LAYER BY OFFSHORE MODIFICATION OF LAND AIR

Earl E. Gossard

NOAA/ERL/Wave Propagation Laboratory
Boulder, Colorado 80303

ABSTRACT

The usual picture of the development of temperature and humidity boundary layers in a land air mass that moves offshore is shown to be very wrong under one type of Foehn condition in southern California, and it is probable that similar conditions can prevail in widespread areas around the globe, notably the Mediterranean Sea and the monsoonal regions of the Near East and Southeast Asia. A formalism is developed for analyzing the modification that seems to represent the observations satisfactorily, and graphical solutions for radio and optical ducting are given. It is shown that offshore modification can lead to elevated layers rather than surface based layers, and the height of the layer base is theoretically predicted. Values of evaporation and heat flux into such an air mass are calculated and the distance offshore at which dew point depression becomes zero is predicted. A method for measuring the downward heat flux in elevated inversion layers is described and results are given.

Background

Many of the oceanic coastal areas of the world are subject to land-sea circulation patterns that lead to spectacular refractive effects at both optical and radio frequencies. These effects often result from (e.g., Richter et al., 1979) the contrast between the temperature and humidity at the sea surface and the temperature and humidity of the overlying air whose origin was over adjacent land

areas. The refraction and ducting resulting from the air-sea contrast in refractive index has usually been discussed under the name "evaporation duct." This type of ducting was originally observed and described by Katzin et al. (1946) and has been analyzed and measured since by Anderson and Gossard (1953), Jeske (1965), and Richter and Hitney (1975). The mechanism of generation of the duct, and analytical approaches to its formation in the neighborhood of coastlines have been given by Gossard (1978) where analytical results were compared with measurements by Craig (1946). In Fig. 1 of this paper we show similar measurements made during the Canterbury Project in New Zealand. Boundary layers such as that shown in Fig. 1 and those measured by Craig are formed by relatively straightforward evaporative diffusion of moisture (and heat) within a boundary layer in which the initial temperature profiles, over the coastal areas, are nearly neutral and the profiles in the boundary layer approximate classical functions such as the log-linear, Monin-Obukov distribution. The presence of a duct, its thickness and intensity should then be readily predictable if the sea temperature and the temperature and humidity of the air at some height (say bridge height) are known or predictable. The various relationships to be expected for power-law and log-linear profiles are given by Gossard (1978). The relationships are satisfactorily borne out by measurements at Key West and during some seasons in the eastern Mediterranean.

However, the predicted relationships fail badly off southern California. In 1955, the author and L. J. Anderson operated a variable height radar on the coast of Pt. Loma at a small height above the sea using targets of known crossection on San Clemente Island and a Coronados Island. The prediction of ducting based on sea and air temperature over the path failed badly and caused a program for incorporation of duct prediction into fleet procedures to be abandoned. In 1971 a more complete and controlled experiment was initiated using an offshore oceanographic platform 1.3 km off the coast as shown in Fig. 2. A track extending from the sea surface to a height of 20 meters was mounted on the platform and was tranversed by an instrumented boom (see Fig. 3). Receivers were raised and lowered continuously through the marine boundary layer at Pt. Loma (Richter (ed.) 1979). Again, the simple relationships between boundary layer meteorological parameters and radio ducting generally failed seriously. However, the experiment provided considerable insight into the reasons for the failure and this is the subject of the present paper. It predicts that the failure may be fairly general in some areas of the world and suggests new predictive relationships that may be applicable.

An example of the spectacular refraction/ducting effects that commonly occur in this area is shown by the photograph in Fig. 4 in which two image inversions of an over-the-horizon vessel are seen. The photograph was taken by R. P. Rogers at the oceanographic platform shown in Figs. 2 and 3. The corresponding profiles of humidity and refractive index measured at the platform taken at 1040 PST using a dewpointer on the boom are shown in Fig. 5. Although conditions such as these are common in southern California, as evidenced by the well known distortions of the solar limb as the sun sets, it is rare to find the transition between the marine layer and the overlying air so low that the profile can be measured in detail through the discontinuity by means of an instrumented tower. Therefore, this case warrants special examination.

The nearest RAWIN in space and time was the 0400 PST sounding taken at Montgomery Field about 11 km inland at an elevation of 124 m MSL. The low-level sounding data are shown in Table 1. The corresponding surface weather map is shown in Fig. 6 and the plot of potential temperature, lowered adiabatically to sea level, is shown in Fig. 7 (solid curve). Clearly, the lower troposphere was extremely stable as is typical of the northeasterly circulation pattern revealed by the weather map under the Foehn condition known locally as a Santa Ana. Such a thermally stable initial profile of temperature produces a model that differs importantly from the cases treated by Gossard (1978) and is the subject of the remainder of this paper.

The Model

The model to be treated here is shown in the top frame of Fig. 8 in which the various symbols are defined. A dry very stable subsiding air mass flows from the interior at constant speed out over the warm coastal waters. In the case analyzed, the surface temperature of the land air was cooler than the water surface temperature (15°C), so a slightly unstable surface boundary layer forms as the air moves out to sea. Because of the stability of the air aloft, the convective boundary layer is capped by a very sharp inversion (Fig. 5) leading to spectacular optical effects (Fig. 4). For comparison, the model in which the initial profile is neutral is shown in the lower frame. The initial potential temperature profile is θ_o with surface value θ_{os}; the modified profile is θ_1 below δ with

surface value θ_s; above δ the profile is θ_2 with the limiting value above the boundary layer assumed for simplicity to have the constant value θ_3. Of course, the assumption of constant sea surface temperature in this area and constant wind over these distances is a rather unrealistic idealization, but the agreement of the calculated inversion height and modified temperature profile 3 km off shore at the oceanographic tower, suggests this model may contain the proper basic physics.

In formulating the problem we will use the flux integral method (Gossard, 1953, 1978), an adaptation of the momentum integral used by von Karmen in his analysis of the growth of boundary layers around airfoils (see e.g., Durand, 1935). Thus, if $F_s = \overline{w'\theta'}$ is the vertical flux of temperature from the surface into the airstream,

$$\int_0^x F_s \, dx = \int_0^{\delta(x)} u[\theta_1(z) - \theta_2(z)]dz \tag{1}$$

where $\delta(x)$ is the mixing depth. The integral on the right is represented by the shaded area in the top frame of Fig. 8.

A convenient profile to assume for $\theta_2(z)$ is

$$\theta_2 - \theta_{os} = (\theta_3 - \theta_{os})(1 - e^{-z/h}) \tag{2}$$

where h is the scale height of the profile. The value of h prior to modification by over-water passage is h_o. Profiles for h_o = 50, 100, 300 m are shown superimposed on the RAWIN profile in Fig. 7. In our calculations we will assume h_o = 100 m, a compromise between the $h_o \simeq 200$ suggested by Fig. 7 and the much smaller h_o suggested by Fig. 5.

A convenient profile to assume for $\theta(z)$ is the power law

$$\theta - \theta_s = (\theta_\delta - \theta_s)\left(\frac{z}{\delta}\right)^m . \tag{3}$$

The log-linear is a physically more satisfactory profile, but it is mathematically awkward, and it can be easily related to a reasonable power law as shown in Fig. 9 in which the radio duct thickness in the boundary layer is compared for the two functional forms.

The measured wind at the tower was light and variable averaging 0.5 m s^{-1} at the time of the observations shown in Figs. 4 and 5. In the calculations, u will be assumed to be 0.5 m s^{-1} over the path from shore and over the height interval of the surface layer. The integral on the right-hand side of eq. (1) then shows the flux of heat (temperature) upward from the surface, F_s, as

$$\bar{u}_1 \frac{d}{dx} \left[(\theta_s - \theta_\delta) \frac{1}{m+1} \delta - (\theta_3 - \theta_\delta)\delta + h(\theta_3 - \theta_{os})(1 - e^{-\delta/h}) \right] = F_s . \qquad (4)$$

where $\bar{u}_1$ is the height-averaged wind below δ, and is assumed to be constant with x. It is convenient to express the surface flux F_s in terms of the drag coefficient C_d defined in relation to the vertical velocity flux $\overline{u'w'} = F_u$ as

$$F_u = - \frac{1}{2} C_d \bar{u}_1^2 .$$

$$F_s = F_u \frac{\theta_\delta - \theta_s}{u_\delta} P_r^{-1} \qquad (5)$$

where P_r is the ratio of the eddy coefficients of momentum and heat, usually assumed to be about unity under approximately neutral conditions; so, assuming $u_\delta \simeq \bar{u}_1$,

$$F_s \simeq - \frac{1}{2} C_d \bar{u}_1 (\theta_\delta - \theta_s) . \qquad (6)$$

[In this formulation it is noteworthy that $\bar{u}_1$ cancels from both sides of Eq. (4).] However, because the initial value of θ was the height-varying profile $\theta_o(z)$, θ_δ is not constant with distance, i.e., it depends on x through δ. The two can be related through the down-gradient flux of heat, F_A, above $\delta(x)$.

So far we have considered only the effect of the upward flux of heat, F_s, from the sea surface that warms the lower layers of the air during its over-water

passage. However, there is a down-gradient heat flux aloft, F_A, above the mixed layer depth, δ. The spectacular optical effects and the virtually complete discontinuity in the height gradient of temperature at δ shown in Fig. 5 suggest little shear at the height of the discontinuity and negligible entrainment of heat across the interface. Then, analogous to eq. (4)

$$\bar{u}\,\frac{d}{dx}\int_{\delta(x)}^{\infty}[\theta_2(z) - \theta_o(z)]dz = F_A\,, \tag{7}$$

where $\bar{u}$ is wind speed above δ and is independent of x.

$$F_A = \bar{u}_2\,\frac{d}{dx}\,[h(\theta_3 - \theta_\delta)] \tag{8}$$

whence

$$\frac{h}{h_o} = \left[e^{-\delta/h_o} - \frac{F_A(x/h_o)}{\bar{u}(\theta_3 - \theta_{os})}\right] e^{\delta/h} \tag{9}$$

where x has its origin at the coastline. Equation (2) gives

$$\theta_\delta = \theta_{os} + (\theta_3 - \theta_{os})(1 - e^{-\delta/h(x)}) \tag{10}$$

where h(x) is given by (9). Substituting (10) in (4) and taking the indicated derivatives, we obtain the ordinary differential equation

$$\left[\frac{m}{m+1}\left(B + \frac{1}{m}\,\frac{\delta}{h}\,e^{-\delta/h}\right) + D\,\frac{1-e^{(\delta/h)(1-h/h_o)}}{1+\frac{\delta}{h}}\right]\frac{d(\delta/h)}{d(x/h)} - \frac{D\,F_A}{\bar{u}(\theta_{os}-\theta_3)e^{-\delta/h}(1+\frac{\delta}{h})} - \frac{C_d}{2}\,B = 0 \tag{11}$$

where

$$B = \frac{\theta_s - \theta_{os}}{\theta_3 - \theta_{os}} - (1 - e^{-\delta/h}) \tag{12}$$

$$D = 1 - e^{-\delta/h} - \frac{\delta}{h}\,e^{-\delta/h} - \frac{\delta^2}{h^2}\,\frac{e^{-\delta/h}}{m+1}\,.$$

The Fluxes F_s and F_A

For convenience we have chosen to express the flux F_s in terms of the drag coefficient C_d. For a smooth sea Sheppard finds $C_d = 3.8 \times 10^{-3}$ (see Sutton, 1949). Therefore, we will assume a value of $C_d = 3.8 \times 10^{-3}$ and also compare the results with a value an order-of-magnitude greater; i.e., $C_d = 3.8 \times 10^{-2}$.

Direct observations of F_A do not exist but we will show that it can be inferred from the type of observation made Ochs and Lawrence (1972) in the San Diego area. An example of the Ochs-Lawrence observations is shown in Fig. 10 where C_θ^2 is the structure constant of temperature. A fairly fundamental relationship between structure constant, turbulent dissipation rate, ε, and rate of destruction of temperature vairance, ε_θ, is (Corrsin, 1951)

$$C_\theta^2 = \alpha^2 \varepsilon^{-1/3} \varepsilon_\theta \tag{13}$$

where α^2 has sometimes been chosen to be 2.8 (Ottersten, 1969). On the other hand, defining ε_θ as dissipation rate of half the variance, Wyngaard et al. find $\alpha^2 = 3.2$ from an experiment at Liberal, Kansas. For present purposes we adopt the Wyngaard convention. Then

$$\varepsilon_\theta = - \overline{w'\theta'} \frac{\partial \theta}{\partial z} - \frac{1}{2} \frac{\partial}{\partial z} \overline{\theta'^2 w} \tag{14}$$

where w is vertical velocity, primes denote perturbation quantities and overbars indicate an average. In stable portions of the atmosphere, such as the region above δ in our model, the first term on the right-hand side of (13) dominates the second (e.g., Lumley and Panofsky, 1964), so the temperature flux

$$\overline{w'\theta'} \simeq - \frac{1}{3.2} C_\theta^2 \varepsilon^{1/3} \left(\frac{\partial \theta}{\partial z}\right)^{-1} . \tag{15}$$

An important fact to note is that ε is raised to a small power (1/3) so it need not be measured or estimated with great accuracy. An order of magnitude error

in ε causes only a factor of 2 error in temperature flux. Observations of velocity variance within stable inversion layers have been reported by Gossard et al. (1978), and the variance has been converted to ε using an analytical development by Frisch and Clifford (1974). Within the inversion layer a value of ~ 30 cm^2 s^{-3} was found. However, an error of a factor of 2.87 in a constant used by Frisch and Clifford has been pointed out by several workers. (Their "A" should be (.47) (55/18) instead of 0.47). Therefore, the ε found by Gossard et al. in the inversion should have been $\varepsilon \simeq 10$ cm^2 s^{-3} which will be used here in our flux estimates. The data collected by Ochs and Lawrence have been tabulated in Table 2. The results of plotting the average flux profile for their seven San Diego flights are shown in Fig. 11 where the number of points averaged in the height intervals are indicated by the circled numbers. The height, z, has been normalized to the height of the inversion base z_i. If, instead of averaging points in height intervals, the average maximum (negative flux and average height of the maximum were taken, it is found that $\overline{w'\theta'}_{max} = 5.7 \times 10^{-3}$ and $\bar{z}/z_i = 1.02$. Most of the Ochs/Lawrence data were collected in the southern California subsidence inversion that often caps the marine boundary layer in that area. The data suggest the temperature fluxes in such layers to be about one fourth of the fluxes to be expected in midwest frontal situations. In calculating the flux magnitudes, it was assumed that $\varepsilon \simeq 10$ cm^2 s^{-3}. For present purposes we will assume $F_A = -0.002$ deg m s^{-1} and also the much larger value of -0.04 deg m s^{-1} for comparison.

Results of the Model

Based on the above analysis, we assume for the model calculations that

$$C_d = 3.8 \times 10^{-3},\ 3.8 \times 10^{-2}$$

$$F_A = -0.04 \text{ deg m s}^{-1},\ -0.002 \text{ deg m s}^{-1}.$$

From Figs. 5 and 7, we choose

$$\theta_{os} = 12.6°C$$

$$\theta_s = 15°C$$

$$\theta_3 = 28.8°C.$$

The weather information from the oceanographic platform at 1000 PST was

weather	broken high clouds
visibility	15 mi
sea	smooth with slicks
water	very clear
swell	0.5 m height, 12 s period
wind	1 knot (0.5 m s^{-1}) at 025° true N; Height, 20 m

The air trajectory from the coast based on the local wind information is shown on Fig. 2 as the dashed line from coast to tower. The corresponding overwater path gives a travel time from the coast of roughly 2 hours and

$$x \simeq 3 \text{ km}.$$

Assuming a Monin-Obukov length of $L \simeq -100$ we find from Fig. 9 that $m \simeq 0.05$ if duct thickness d is chosen as a criterion for matching.

To aid in choosing an appropriate value for the initial scale height, h_o, we have plotted exponentials on the sounding data in Fig. 7 corresponding to h_o = 50, 100, 300 m. We have chosen h_o = 100 as a best compromise between a fit to the sounding and the much smaller h suggested by the region above δ in Fig. 5.

The results plotted from eqs. (2a), (3) and (10) are shown in Figs. 12, 13, 14 and 15 for $C_d = 3.8 \times 10^{-3}$ and for F_A = -0.002 and -0.04. The pattern revealed in Fig. 12 is a good representation of the observations shown in Fig. 5 considering the uncertainties in the initial profile obtained from a RAWIN at 0400 PST, 11 km inland. The depth of the layer δ is about 10 m at a distance of 3 km and $\theta_s - \theta_\delta = 0.74°C$. Figures 14 and 15 show the result of assuming a larger flux (F_A) aloft than is considered to be typical of this meteorological condition, unless (as is suggested by the surface chart, Fig. 6) it is accentuated by subsidence resulting from divergence in the marine layer.

Having found δ by solution of the differential equation (11), θ_δ can be found from (10) and the heat flux as a function of distance x can be found from (6). It is shown plotted with δ in Figures 13 and 14. If F_A is not zero, there is a cut-off in heat flux a short distance from the coast (46 km) where the potential temperature of the air rises to the sea surface temperature. With the larger F_A assumed in Fig. 14, the cut-off occurs at an x of only 11.9 km from shore. After F_s becomes zero the only remaining flux is the downward flux F_A that slowly lowers δ until some other process, such as entrainment, condensation, radiation or conduction of heat to the sea establishes a different set of balances, or until the temperature of the underlying sea surface changes. A similar pattern is found in evaporation (moisture flux).

Evaporation

The amount of moisture being evaporated into the marine boundary layer under Chinook conditions of this kind can also be evaluated from the data of Fig. 5. Writing a moisture integral analogous to eq. (1), we find

$$\int_0^x E\, dx = \bar{u} \int_0^\delta (q(z) - q_o)\, dz \tag{16}$$

where E is evaporative moisture flux, q is water vapor density in g m^{-3} and the v quantities are defined schematically subscripted in Fig. 16. It is again noteworthy that the transition between the marine air and the land air above is remarkably sharp. From Fig. 5 we note that relative humidity falls from 72% to 50% over a height range of less than 2 meters. The various values of moisture density defined in Fig. 16 are: $q_\delta \simeq 7.5$ g m^{-3} (i.e., $e \simeq 12.2$ mb), $q_o \simeq 5.1$ (i.e., $e \simeq 8.3$) and $q_s = 10.5$. Writing

$$q(z) - q_o = (q_s - q_o) + (q_\delta - q_s)\left(\frac{z}{\delta}\right)^m \tag{17}$$

we find

$$E = u\left[\frac{d}{dx}(q_s - q_o)\delta(x) - \frac{1}{m+1}\frac{d}{dx}(q_s - q_\delta)\delta(x)\right]. \tag{18}$$

For convenience, let

$$q_s - q_\delta = q_s - q_o - Q \tag{19}$$

where $Q = q_\delta - q_o$

so that

$$\frac{d}{dx}(q_s - q_\delta) = -\frac{dQ}{dx} \quad . \tag{20}$$

Analogous to the heat flux, given by eqn. (6), the moisture flux is given by

$$E \simeq 1/2\ C_d\ \bar{u}(q_s - q_\delta) \equiv 1/2\ C_d\ \bar{u}(q_s - q_o - Q) \tag{21}$$

so, eqn. (18) becomes

$$\frac{dQ}{dx} = -(m+1)\left[\frac{Q}{\delta}\left(\frac{C_d}{2} + \frac{1}{m+1}\frac{d\delta}{dx}\right) + \frac{q_o - q_s}{\delta}\left(\frac{C_d}{2} - \frac{1}{m+1}\frac{d\delta}{dx}\right)\right] \quad . \tag{22}$$

Having $\frac{d\delta}{dx}$ from eqn. (11), eqn. (22) can be integrated with Q=0 as the initial condition at the shoreline. From (21), evaporation and dew point depression can then be computed. They are shown on Figures 13 and 15 for two values of F_A. For $F_A = -0.04$ m s^{-1} deg, saturation occurs 12.6 km offshore and for $F_A = -0.002$ it occurs at 46 km. The distance offshore to a fog bank might therefore depend fairly critically on F_A. If $F_A = 0$ saturation would never be quite reached.

In both cases about 13.7 grams are evaporating over the 3 km, one meter wide path from the shore to the oceanographic tower every second. Figures 17, 18, 19, and 20 show, respectively, cases in which the drag coefficient is 0.038 and in which $(\theta_s - \theta_{os})/(\theta_3 - \theta_{os}) = 0.28$ instead of the 0.15 value suggested by the observations on this day. The larger value of $C_d = 0.038$ is probably more typical of sea surface conditions in the area than the order-of-magnitude smaller value used to represent the smooth-glassy sea of the case studied in this paper. The larger ratio of temperature difference was chosen as the largest value considered to be

typical of the California Chinook condition. These values of C_d and temperature difference ratio yield marine layer depths that are more commonly observed in the area than the very thin marine layer of the case studied in this paper.

Radio Ducting

The radio refractive index parameter $N = (n-1) \times 10^6$ (where n is refractive index) is related to temperature and humidity as

$$N = \frac{77.6\ p}{T}\left(1 + \frac{7733\ q}{\rho T}\right) \tag{23}$$

where T is in Kelvin, q is in gr m^{-3} and p is pressure in millibars. A closely related quantity called potential refractive index ϕ is of more direct interest for the present problem because it is defined in terms of potential temperature θ; i.e.,

$$\phi = \frac{77600}{\theta}\left(1 + 7.73R\ q\right) = \frac{77600}{\theta}\left(1 + .022\ q\right) \tag{24}$$

where $R \simeq 2.88 \times 10^{-3}$ is the gas constant and where the equation of state relation $p = \rho RT$ has been used. The moisture density q is in g m^{-3}. In the lower atmosphere radio ducting occurs when

$$\frac{\partial \phi}{\partial z} \leq -0.13 \tag{25}$$

and the thickness, of the duct is the height at which $\partial\phi/\partial z = -0.13$. At that height a ray launched horizontally will bend downward with a curvature equal to that of the earth's (smooth) surface. In our model both θ and q have the functional form of Eq. (2). If h is the same for both, ϕ closely follows the same function, so

$$\phi = \phi_3 - (\phi_3 - \phi_{os})e^{-z/h}$$

and

$$\frac{\partial \phi}{\partial z} = \frac{\phi_3 - \phi_{os}}{h} e^{-z/h} \underset{z=\delta}{=} \frac{\theta_3 - \theta_{os}}{h} e^{-\delta/h} \quad . \tag{26}$$

The function changes its derivative discontinuously at the height δ, so the maximum (negative) gradient of ϕ will occur at the height δ, except for the thin zone of large gradients adjacent to the sea surface. Therefore, if the gradient of ϕ exceeds that given by Eq. (25), a "duct" will exist at the height δ. Figures 21, 22, 23, 24 and 25 give the graphical solution of equations (9), (11) and (26) for use in calculating duct thickness (δ/h) and refractive index gradient ($\partial\phi/\partial z$) assuming the drag coefficient for a smooth sea to be Sheppard's value of $C_d = 3.8 \times 10^{-3}$. The graphical solutions are given in terms of the dimensionless distance x/h_o, modification depth δ/h_o, and scale height h/h_o. They are parametric in $(\theta_s - \theta_{os})/(\theta_3 - \theta_{os})$. It is noteworthy that h_o does not appear in Eq. (11) except in the 2nd term from the left which is about 3 orders of magnitude smaller than the 1st term over the whole range of variables considered here. It is therefore quite negligible in the graphical solution of (11). However, for convenience the plots were non-dimensionalized to h_o rather than h by using Eq. (9).

The reader is here reminded of the constraints on this development:

1) Variations in sea surface temperature and wind are assumed to be independent of x.

2) A height-averaged wind is used in the flux integral. The error from this may be estimated by examining its effect in the special case when θ_2 is constant. Equation (1) may then be readily integrated with $u \propto z^m$. It is then found that $\delta \propto x^{1/(2\,m+1)}$ rather than x^1 as is found when u is constant. When m is very small, such as m = 0.05, the difference is negligible.

3) Entrainment across the interface between the regions above and below δ has been assumed to be negligible, with the balance in fluxes achieved by adjustment of the height δ. Figure 5 suggests that this assumption is justified in the case analyzed in this paper, and therefore it is probably a valid assumption whenever

the stratification conditions are intense enough to cause ducting or to cause the formation of an offshore fog bank.

4) In Figs. 21-24 a value of $C_d = 3.8 \times 10^{-3}$ for a smooth sea has been assumed. If the sea is rough C_d may be significantly larger. However, δ will then be relatively large, and the height gradients at δ will be relatively smaller. Thus radio and optical ducting is not likely and fog or stratus cloud formation will occur farther offshore. Therefore the value of C_d chosen here will probably represent the cases of most interest.

Conclusions

The classical picture of the development of a temperature and humidity boundary layer in a land air mass that moves off-shore can be very wrong in some areas of the world. A formalism is developed in this paper that seems to represent the observational results in a satisfactory way. It is concluded that offshore modification can lead to elevated layers rather than surface based layers in some monsoonal conditions. Values of heat flux and evaporation from the sea surface are calculated and a method for measuring downward heat flux in elevated inversion layers is described. The method may have value in predicting the occurrance of fog and stratus clouds, and predicting the distance to off-shore fog banks.

TABLE 1 (0400 PST RAOB, Montgomery Field)

p (mb)	H (m MSL)	T(°C)	R.H. (%)	Spd (ms^{-1})	Dir
1004 (sfc)	124	12.6	61	2	040
1000	142	18.9	36	2	047
950	586	22.0	18	1	276
900	1052	19.8	16	3	318
850	1541	17.0	15	2	272

TABLE 2

Layers Sounded by Ochs and Lawrence (1972)

Sounding No.	Date	Time	Location	ΔT	h (m)	C_θ^2	$\frac{\Delta T}{h}$	$\frac{d\theta}{dz}_{max}$
1	11 Nov '71	0934	Haswell	2.2	30	1.2×10^{-2}	0.073	.063
2	25 Feb '72	1500	San Diego	5.0	40	1.2×10^{-2}	0.125	0.11
3	26 Feb '72	1200	San Diego	8.0	30	3.5×10^{-2}	0.27	0.34
4	28 Feb '72	1400	San Diego	10.0	40	6.9×10^{-2}	0.25	1.0
5	20 Apr '72	1327	San Diego	1.5	30	1.0×10^{-2}	0.05	0.14
6	20 Apr '72	1840	San Diego	2.8	25	2.3×10^{-2}	0.11	0.11
7	21 Apr '72	1213	San Diego	3.5	17	1.7×10^{-2}	0.20	0.07
8	21 Apr '72	1900	San Diego	5.0	28	2.3×10^{-2}	0.18	0.31

References

Anderson, L.J., and E.E. Gossard, (1953), The effect of the oceanic duct on microwave propagation, Transactions, Amer. Geophys. Union, 34, 695-700.

Corrsin, S. (1951), On the spectrum of isotropic temperature fluctuations in an isotropic turbulence, J. Appl. Phys., 22, 417-423.

Craig, R.A. (1946), Measurements of temperature and humidity in the lowest 1000 feet of the atmosphere over Massachusetts Bay, Papers in Physical Oceanography and Meteorology. Vol. 10, No. 1, Massachusetts Institute of Technology and Woods Hole Oceanographic Institution. Cambridge, Massachusetts.

Durand, W.F. (Editor) (1935), Aerodynamic Theory, Vol. III, Dover Publications, New York, 350 p.

Frisch, A.S., and S.F. Clifford, (1974), A study of convection capped by a stable layer using Doppler radar and acoustic echo sounders. J. Atmos. Sci., 31, 1622-1628.

Gossard, E.E. (1953) The effect of wind on nighttime radiational cooling, Trans. Amer. Geophys. Union 34, 841-848.

Gossard, E.E. (1978) The height distribution of refractive index structure parameter in an atmosphere being modified by spatial transition at its lower boundary, Radio Science 13, 489-500.

Gossard, E.E., R.B. Chadwick, K.P. Moran, R.G. Strauch, G.E. Morrison, and W.C. Campbell (1978), Observation of winds in the clear air using an FM-CW Doppler radar, Radio Science 13, 285-289.

Jeske, H., (1965), Die ausbreitung elektromagnetischer Wellen im cm-bis m-Band über dem Meer unter besonderer Berücksichtigung der meteorologischen Bedingungen in der maritimen Grenzschich, Hamburger Geophysikalische Einzelschriften, De Gruyter and Co., Hamburg.

Katzin, M., R.W. Bauchman, and W. Binnian (1947), 3- and 9-centimeter propagation in low ocean ducts, Proc. IRE, 35 891-905.

Lumley, J.L., and H.A. Panofsky (1964) The Structure of Atmospheric Turbulence, Vol. XII, 222 pp., Interscience, New York.

Ochs, G.R., and R.S. Lawrence (1972) Temperature and C_n^2 profiles measured over land and ocean to 3 km above the surface, NOAA TR ERL 251-WPL 22, 39 pp.

Ottersten, H. (1969) Atmospheric structure and radar backscattering in clear air, Radio Sci., 4, 1179-1193.

Richter, J.H., and H.V. Hitney (1975), The effect of the evaporation duct on microwave propagation, U.S. Naval Electronics Laboratory, San Diego, Calif. Tech. Rept. TR 1949, 31 pp.

Richter, J.H. (Chairman and ed.) (1979) Proceedings of conference on atmospheric refractive effects assessment, Naval Ocean Systems Center, Tech. Doc. 260, 167 p.

Sutton, O.G. (1949) Atmospheric Turbulence, Methuen and Co. Ltd., London 107 p.

Unwin, R.S. (1951) The Canterbury Project, A Radio Meteorological Investigation in the South Island, NZ Vol. 1,2. Published by Dept. Sci. and Indus. Res., Wellington, NZ, 858 p.

Wyngaard, J.C., Y. Izumi, and S.A. Collins, Jr., (1971), Behavior of the refractive-index-structure parameter near the ground, J. Opt. Soc. Amer., 61 1646-1650.

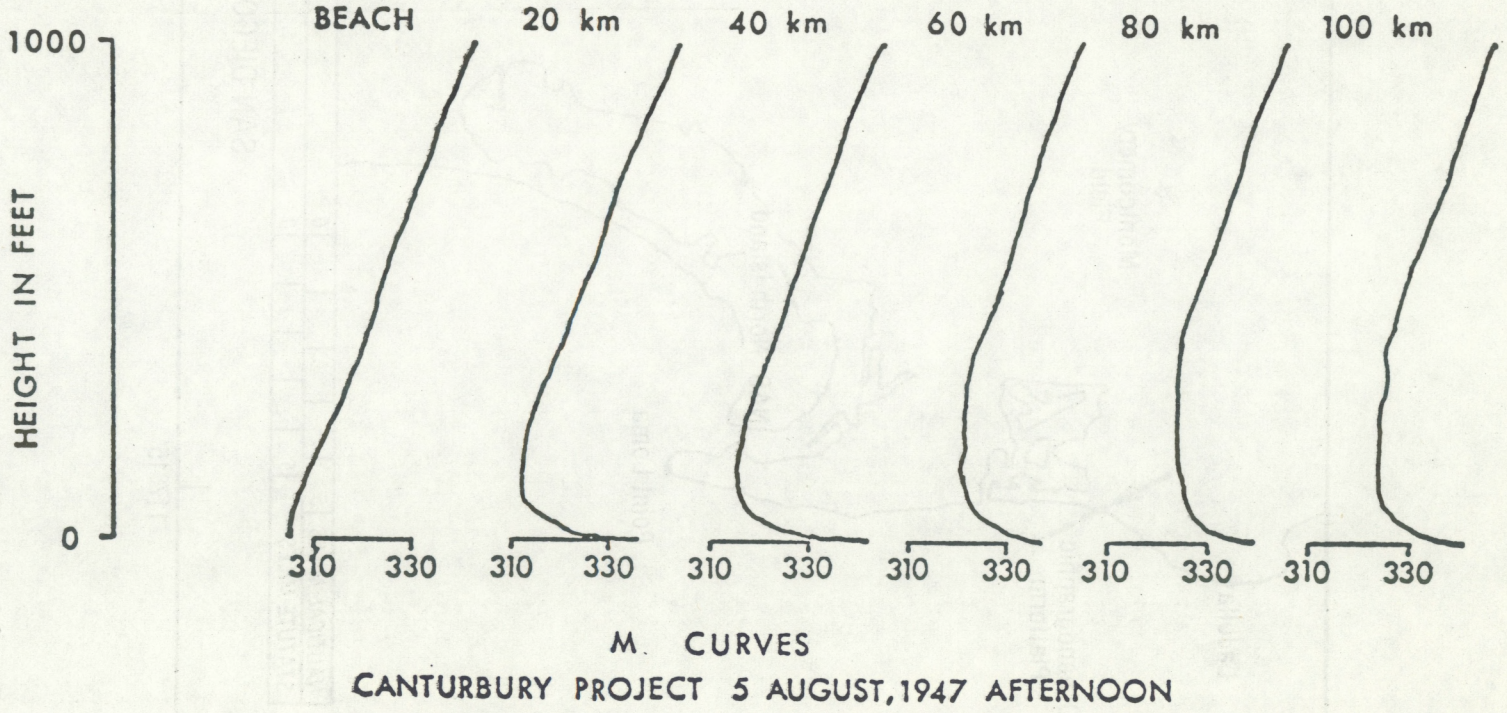

Figure 1. Example of modification of the surface layers of an airmass of neutral stability as it moves offshore the distances indicated. The modified refractive index $M = (n-1) \times 10^6 + 0.157Z$ where n is radio refractive index and z is height in kilometers. Trapping (or ducting) of radio waves occurs where $dM/dz = 0$. Data from the Canterbury Project (Unwin, 1951).

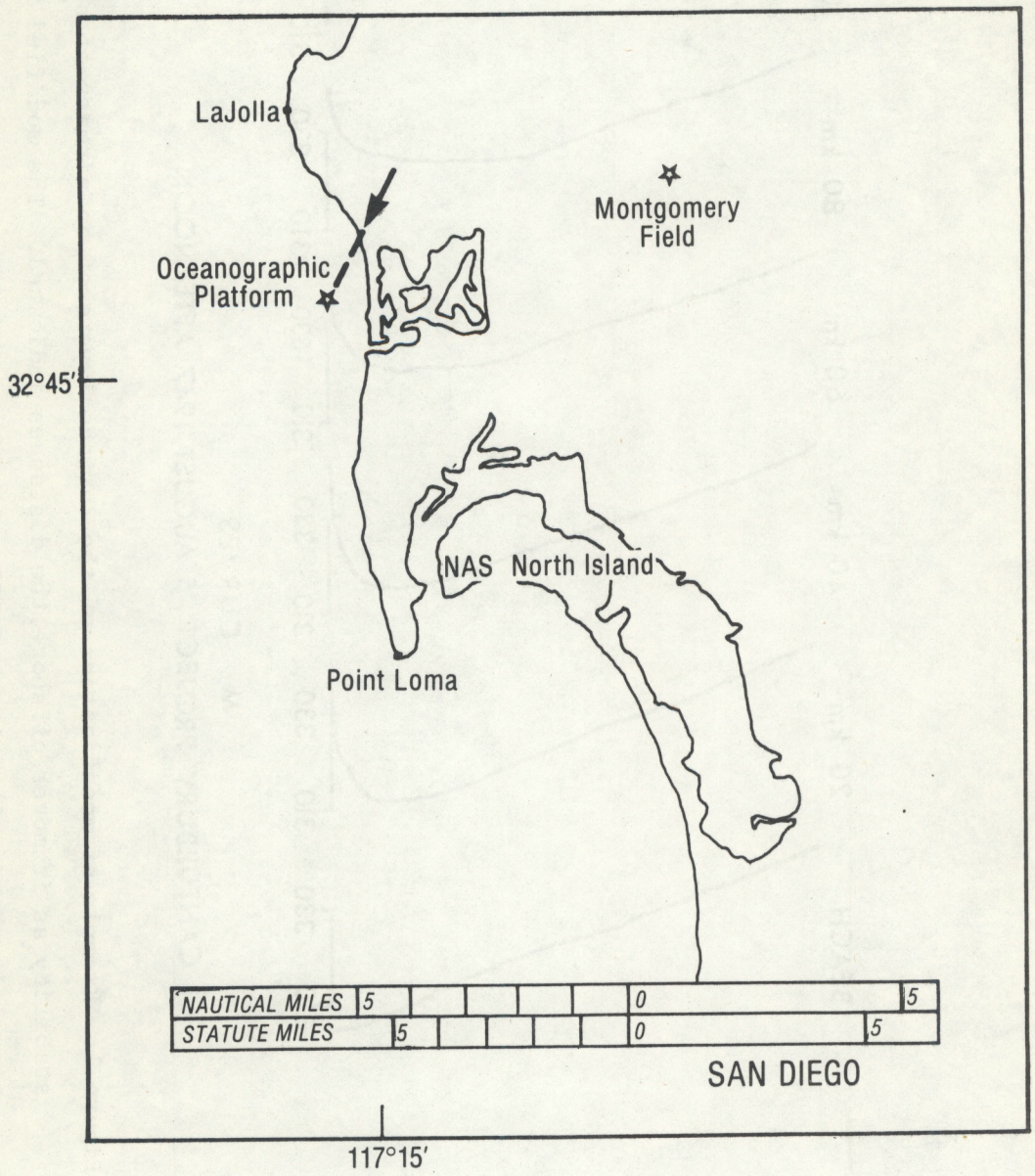

Figure 2. Map of San Diego area showing position of oceanographic platform and air trajectory (dashed line). Raob was released at Montgomery Field.

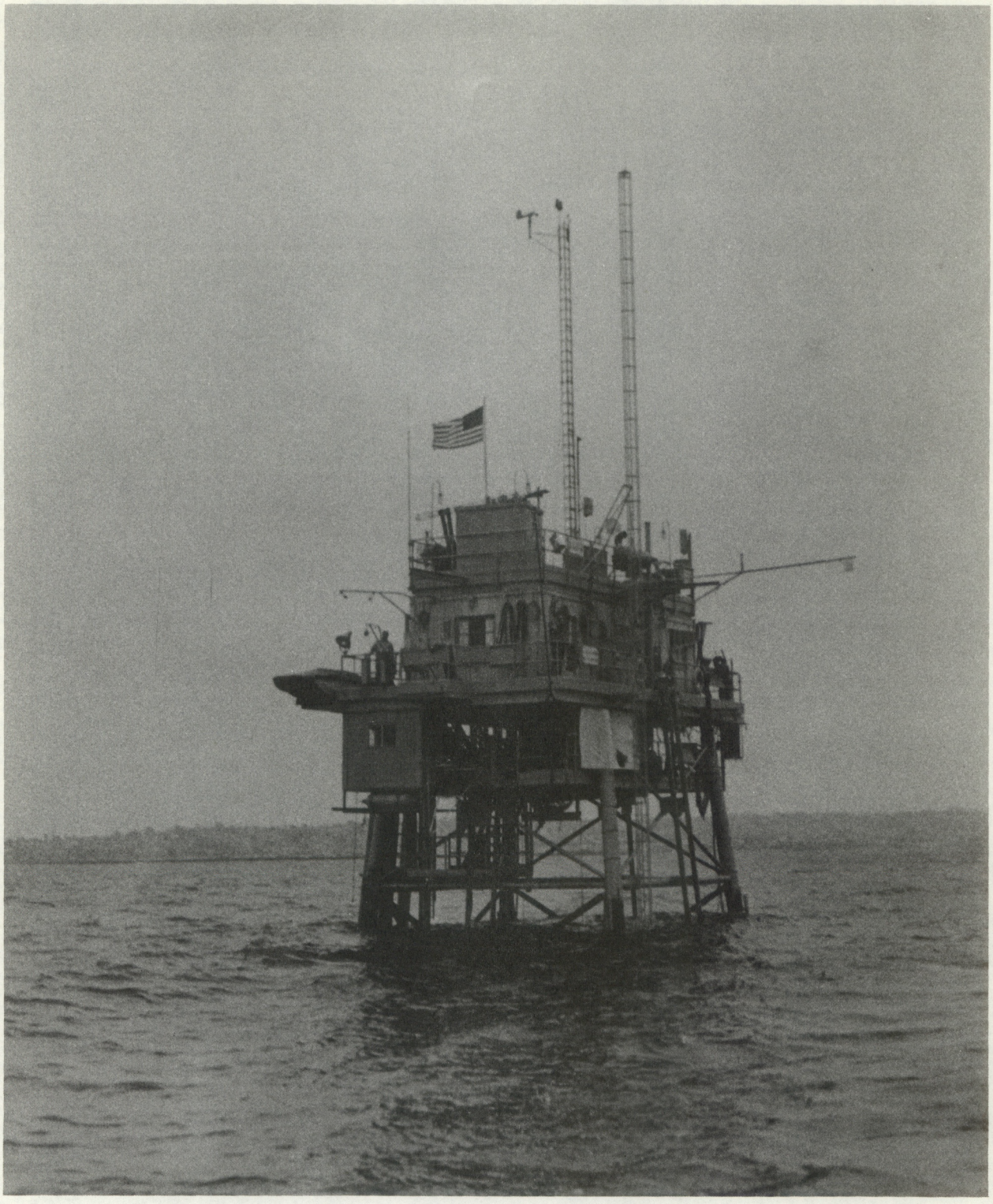

Figure 3. Oceanographic platform showing track and boom with dewpointer on its tip.

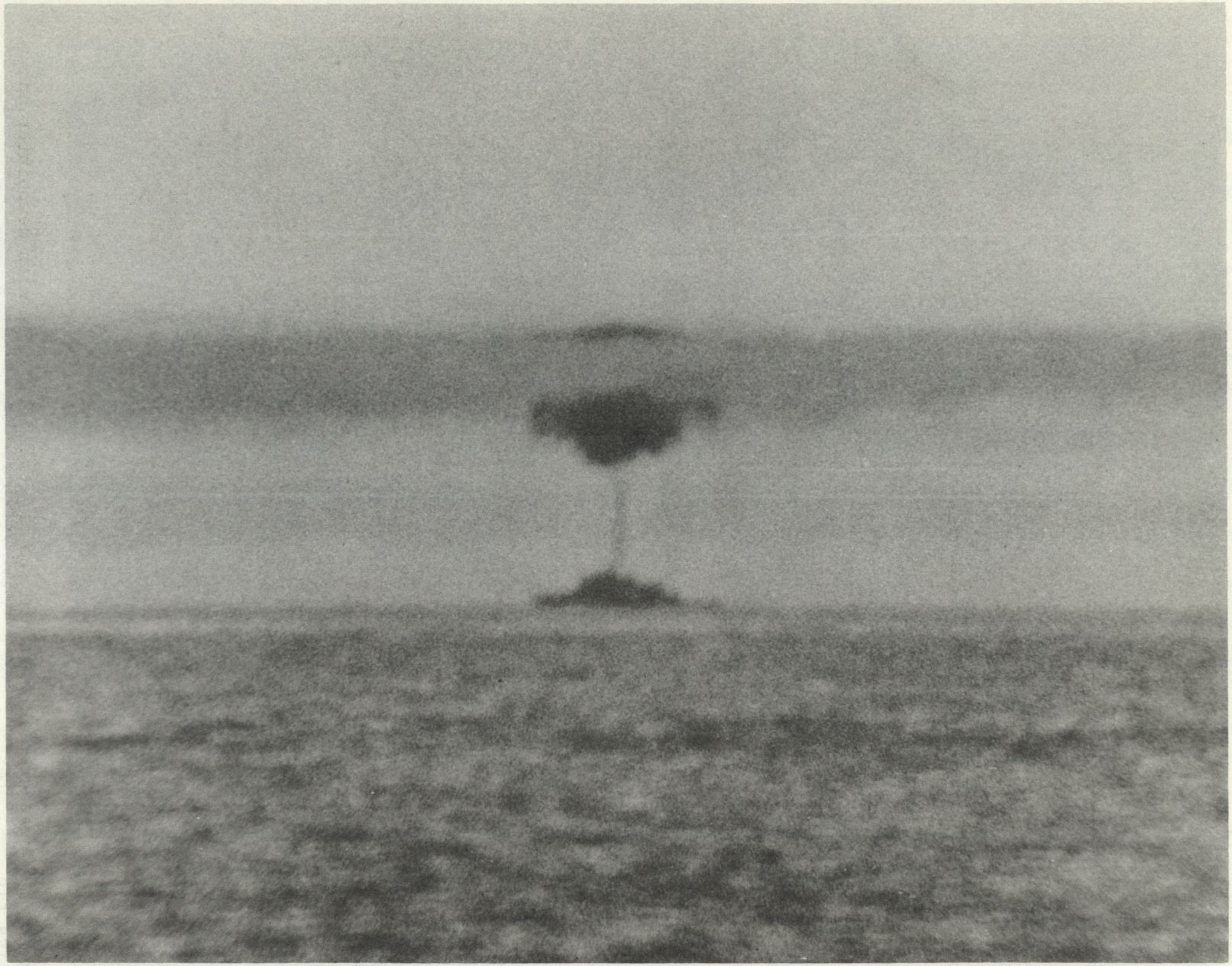

Figure 4. Mirage showing inverted image of boat near horizon (photograph by R. P. Rogers).

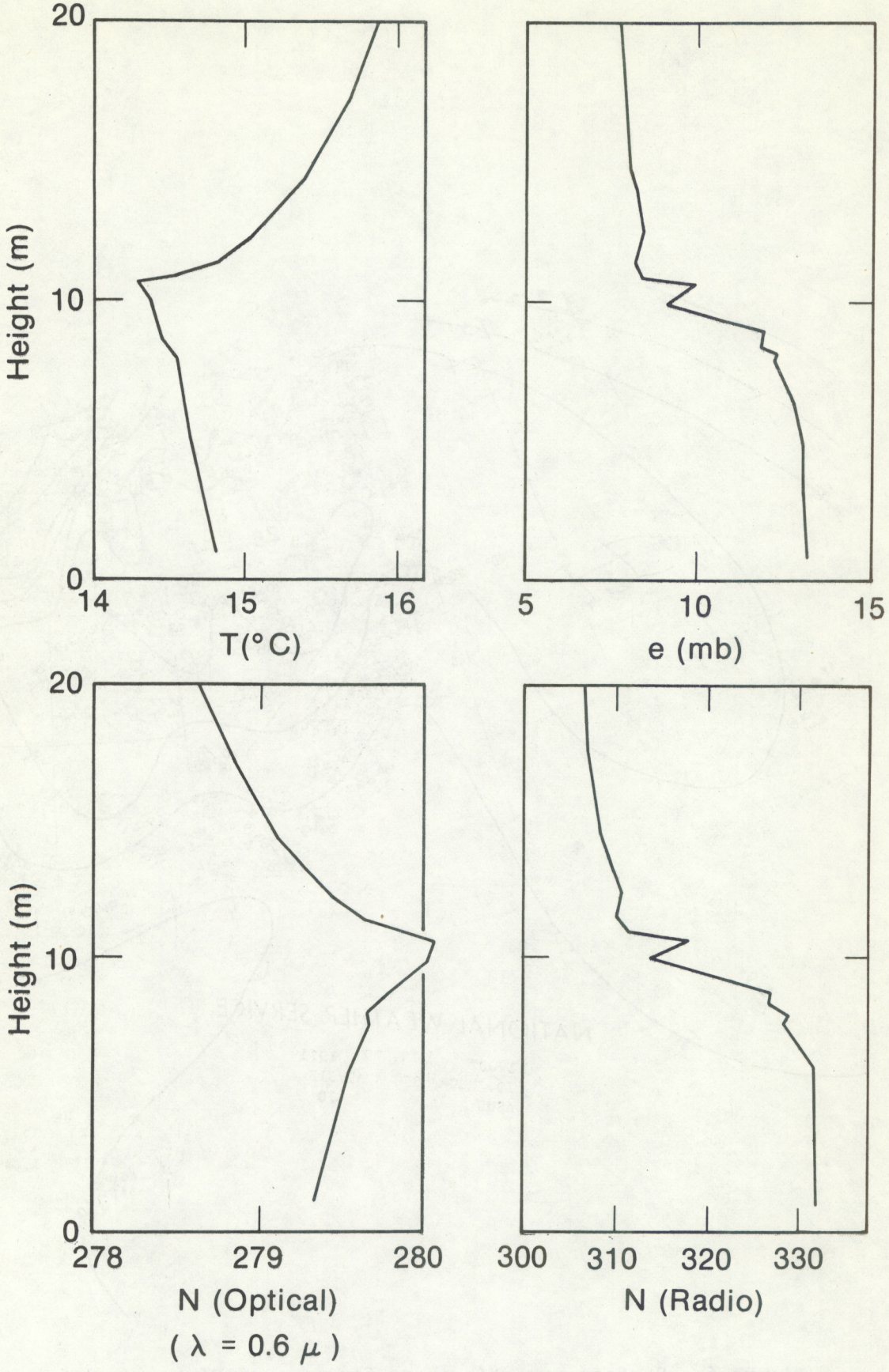

Figure 5. Profiles of meteorological parameters and refractive index at 1040 PST for case shown in Fig. 4.

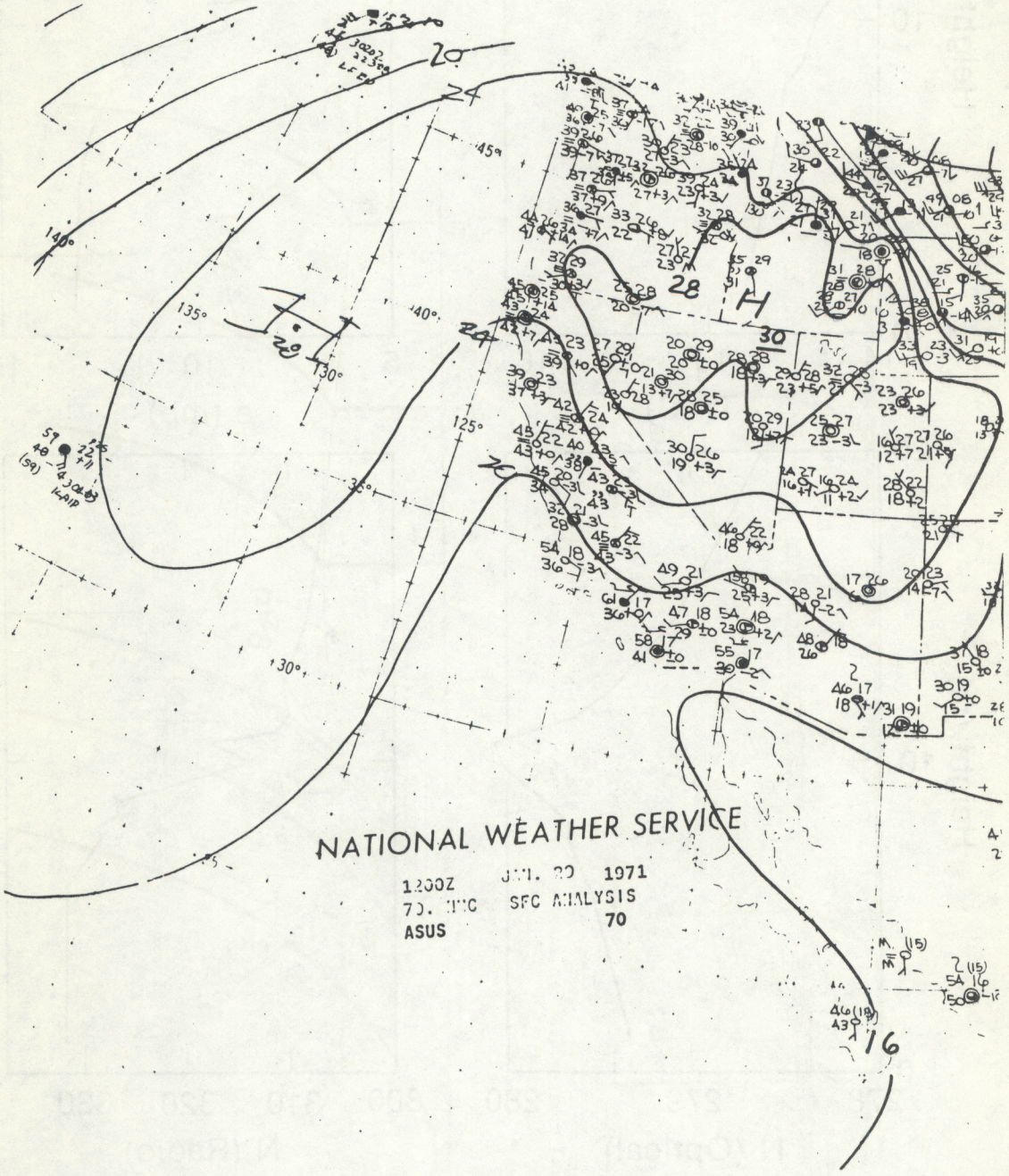

Figure 6. Surface synoptic chart for case of Figs. 4 and 5.

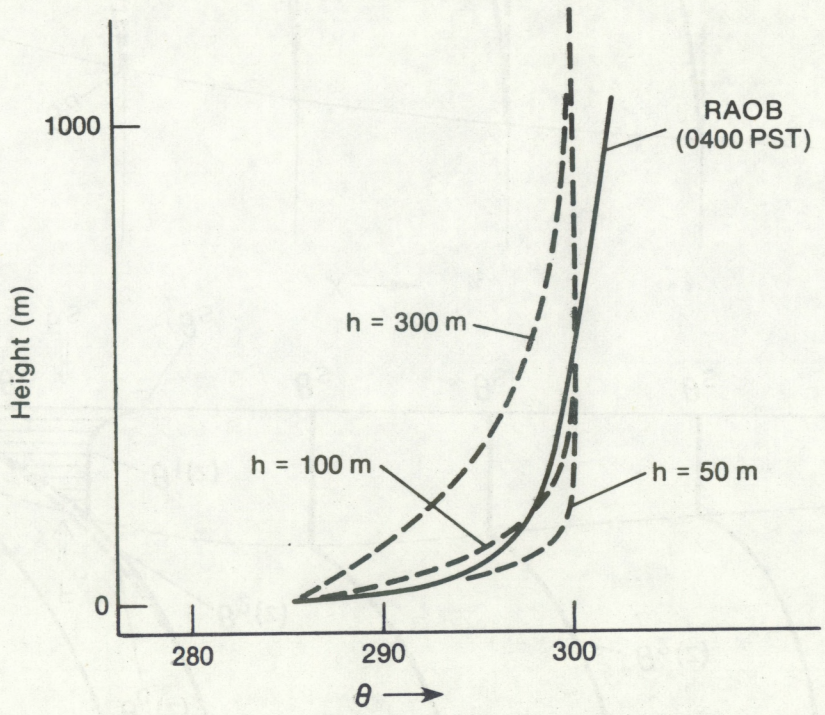

Figure 7. Solid Curve: Morning raob showing profile of potential temperature (lowered adiabatically to sea level from 124 m) and exponential fits to raob assuming various scale heights, h.

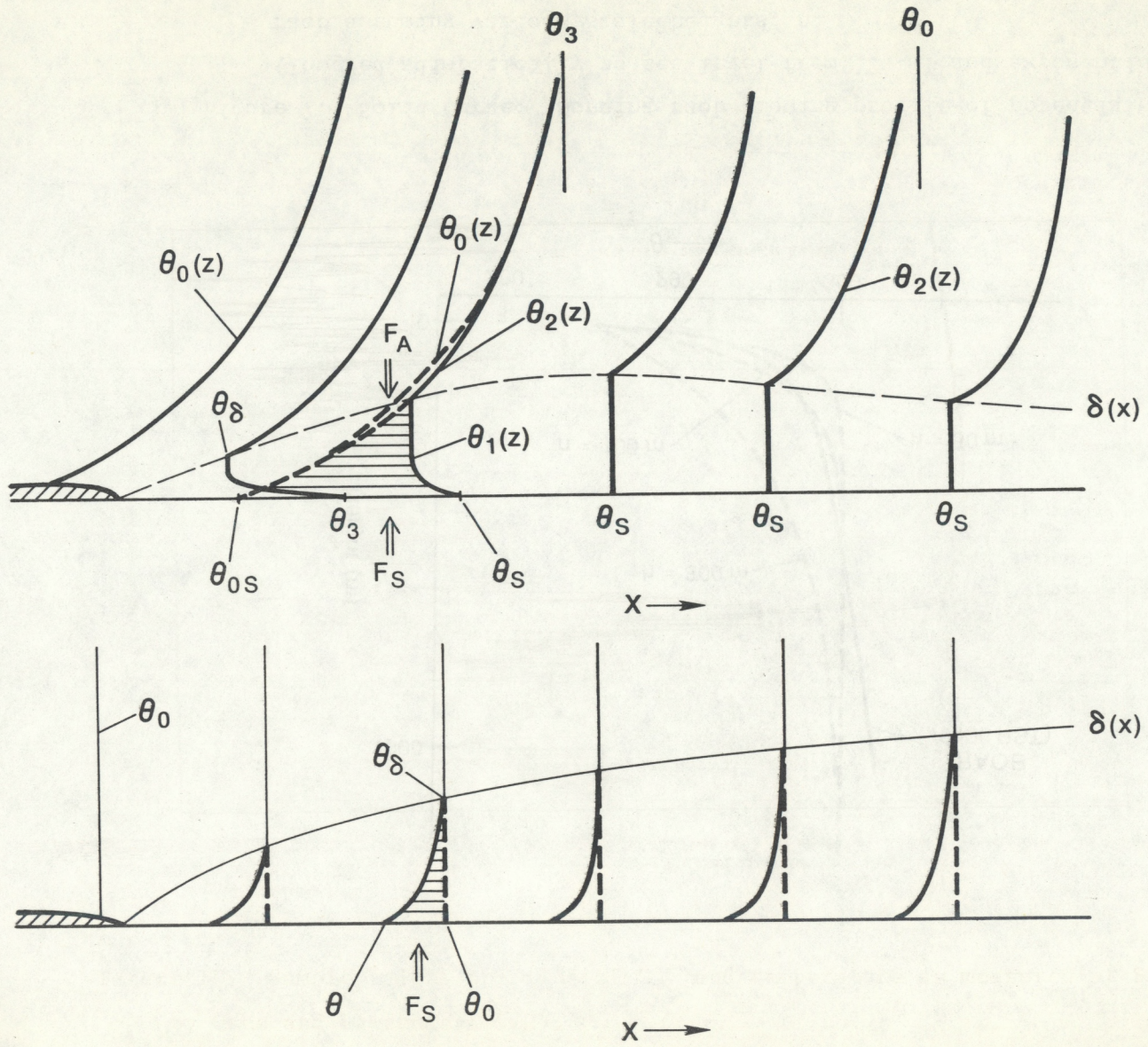

Figure 8. Top frame: Schematic picture of model used in this paper, with definitions.
Bottom frame: Conventional model of off-shore modifications.

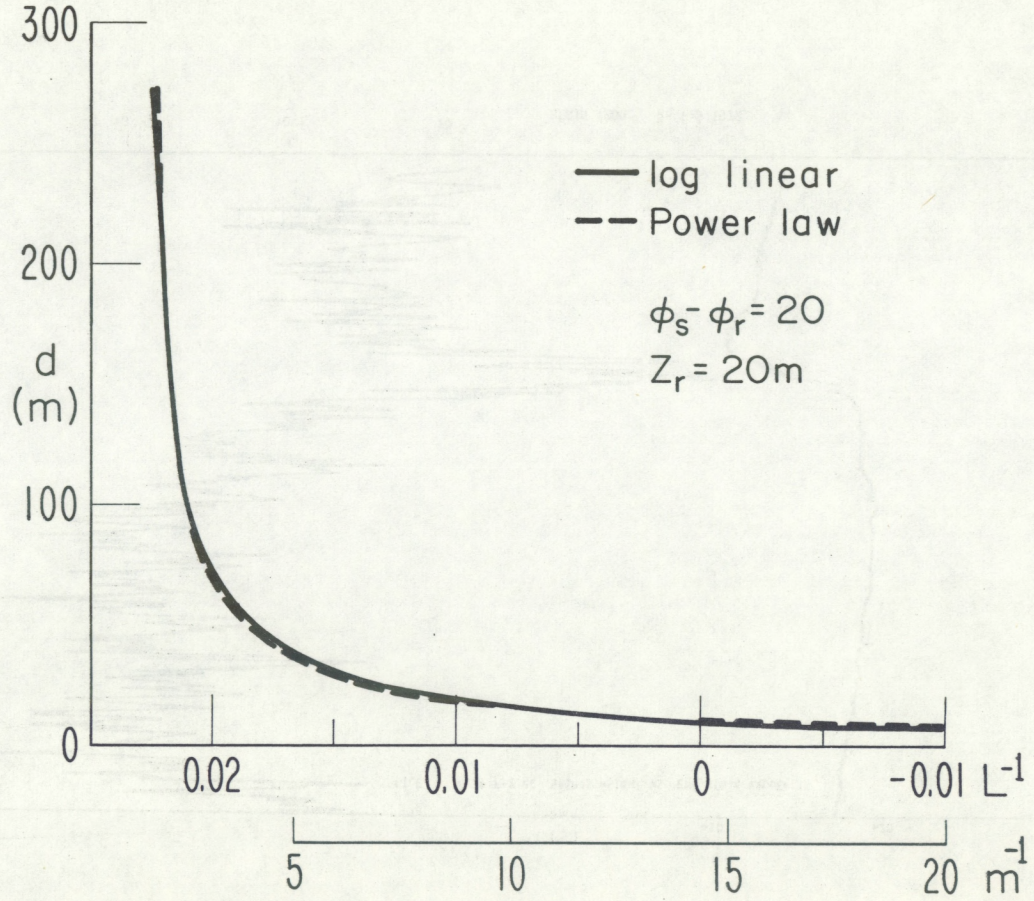

Figure 9. Comparison of duct thickness predictions for log-linear model and power law model for a range of stabilities (L and m).

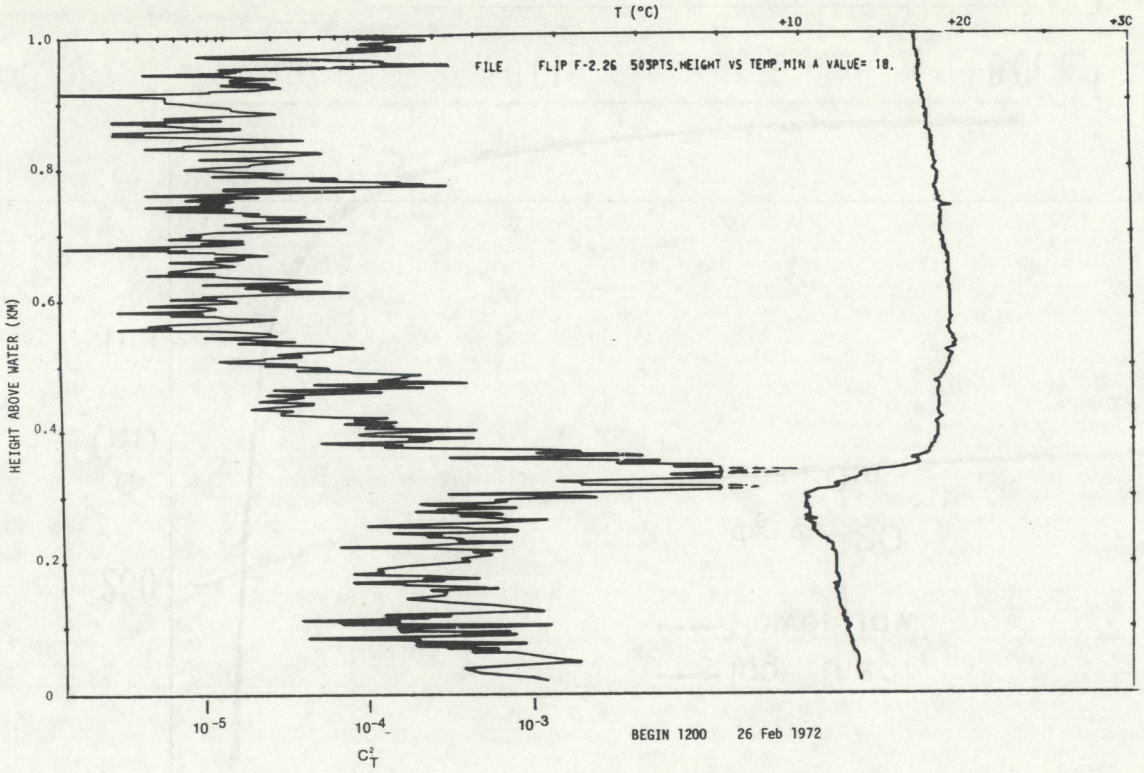

Figure 10. Sample height profiles of C_T^2 and temperature as measured at San Diego by Ochs and Lawrence (1972).

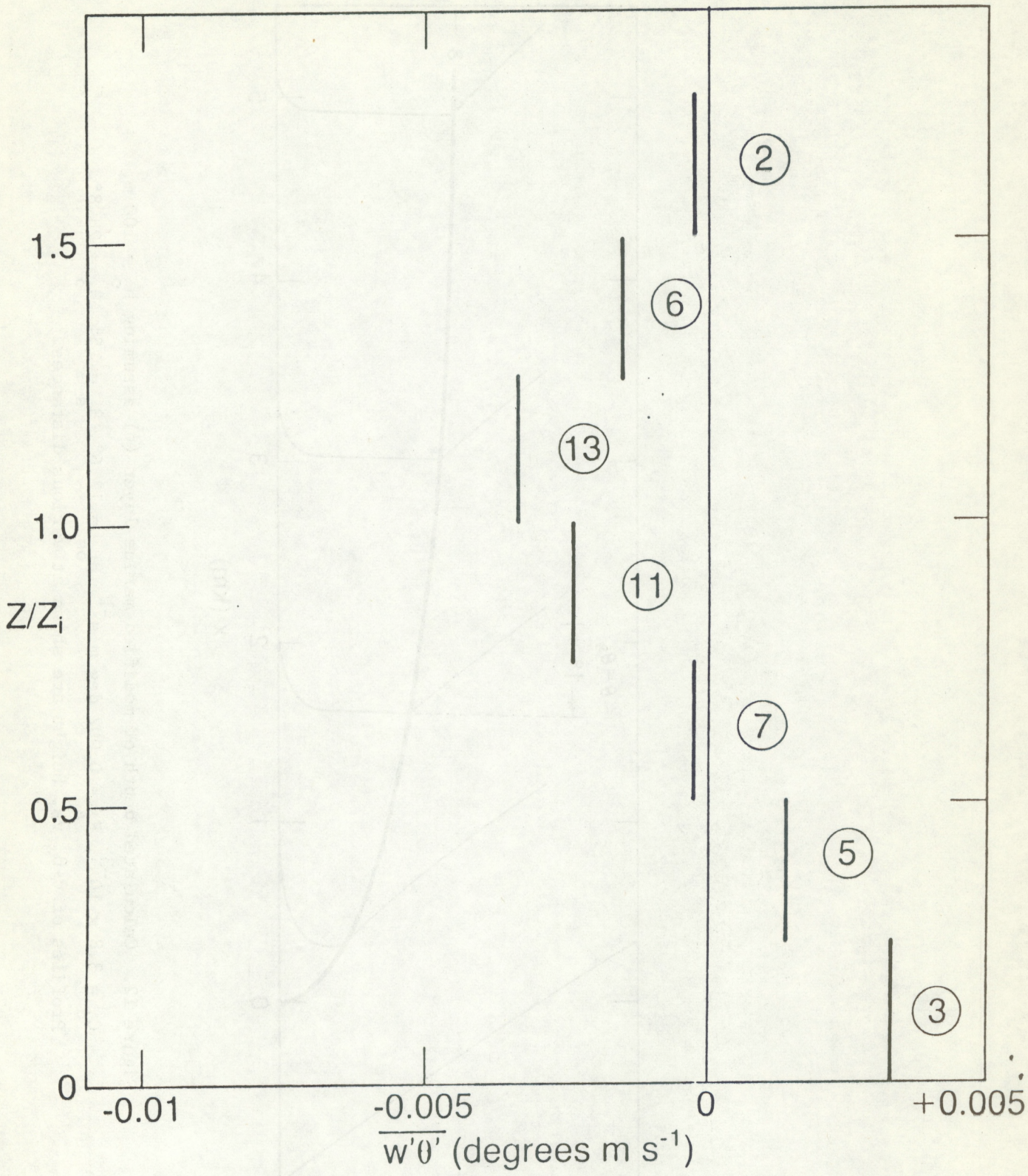

Figure 11. Calculated flux in elevated inversion at San Diego based on the Ochs-Lawrence observations. Numbers in circles indicate flight number. All flights were on different days.

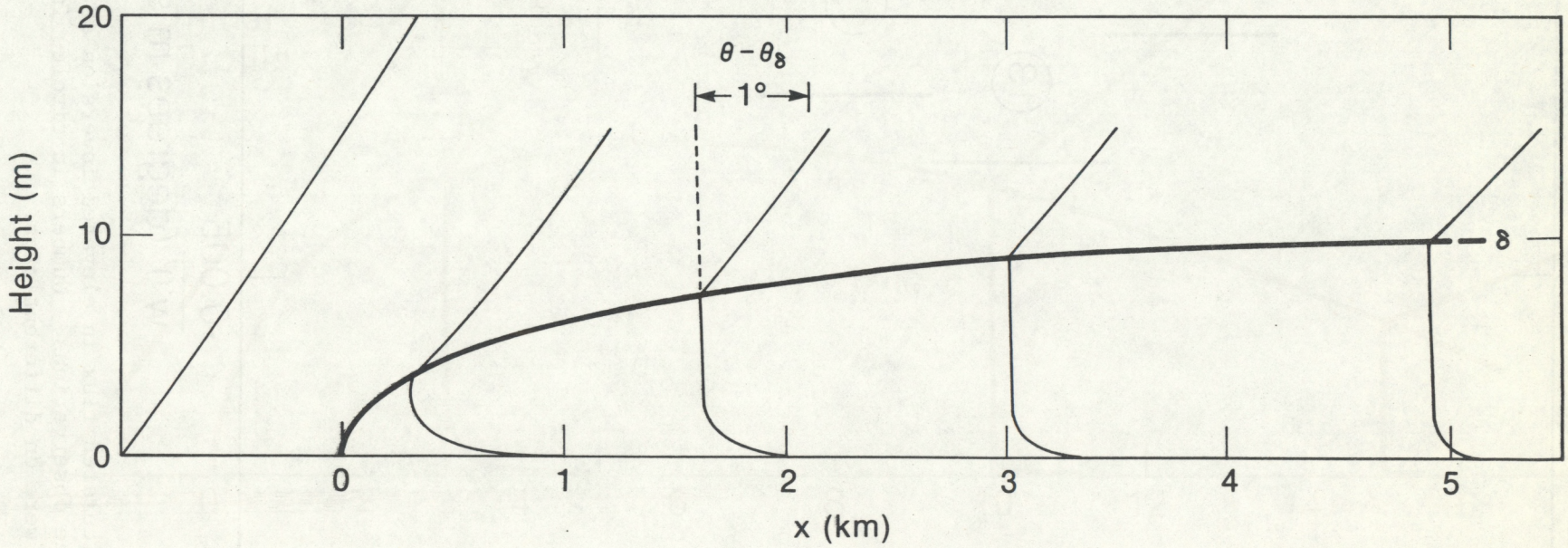

Figure 12. Calculated depth of modified marine layer (δ) assuming h_o = 100 m, $C_d = 3.8 \times 10^{-3}$, F_A = 0.002 deg m s^{-1}, θ_{os} = 12.6°, θ_s = 15°, θ_3 = 28.8°. Profiles of $\theta-\theta_\delta$ vs. height are shown at various distances.

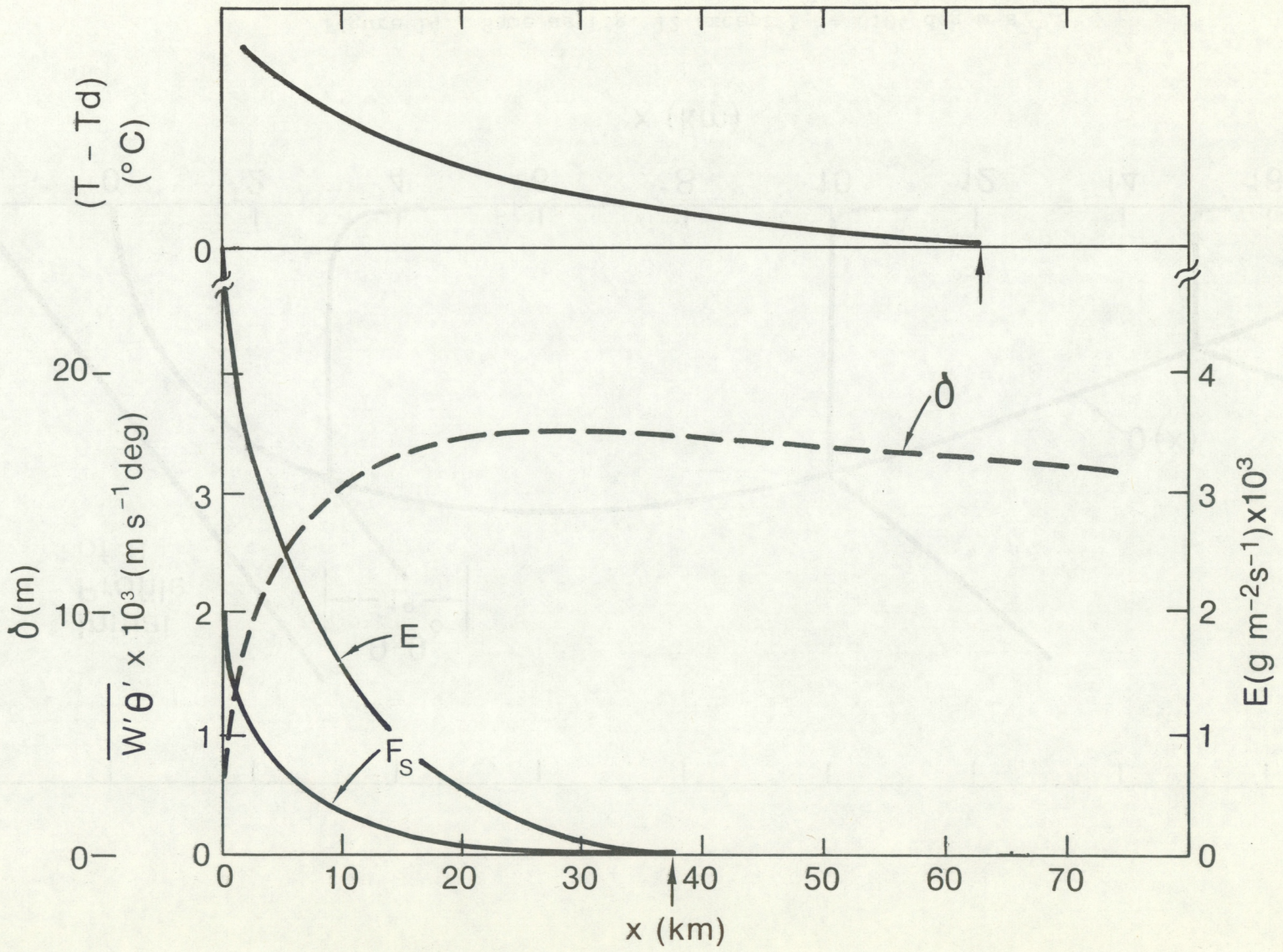

Figure 13. Fluxes of heat and moisture plotted with depth of marine layer and dew point depression as a function of offshore distance x for the case of Fig. 12.

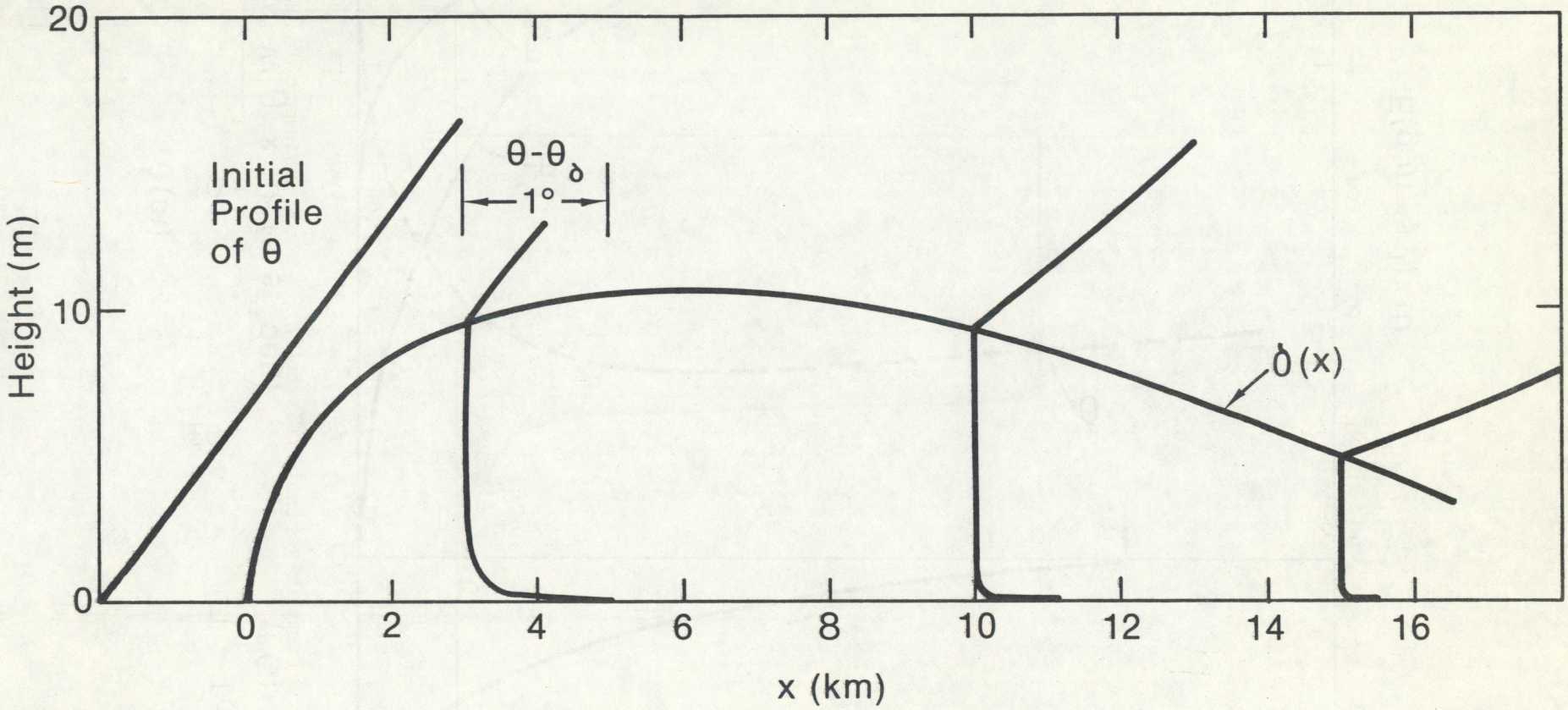

Figure 14. Same as Fig. 12 except F_A = 0.04 deg m s^{-1}.

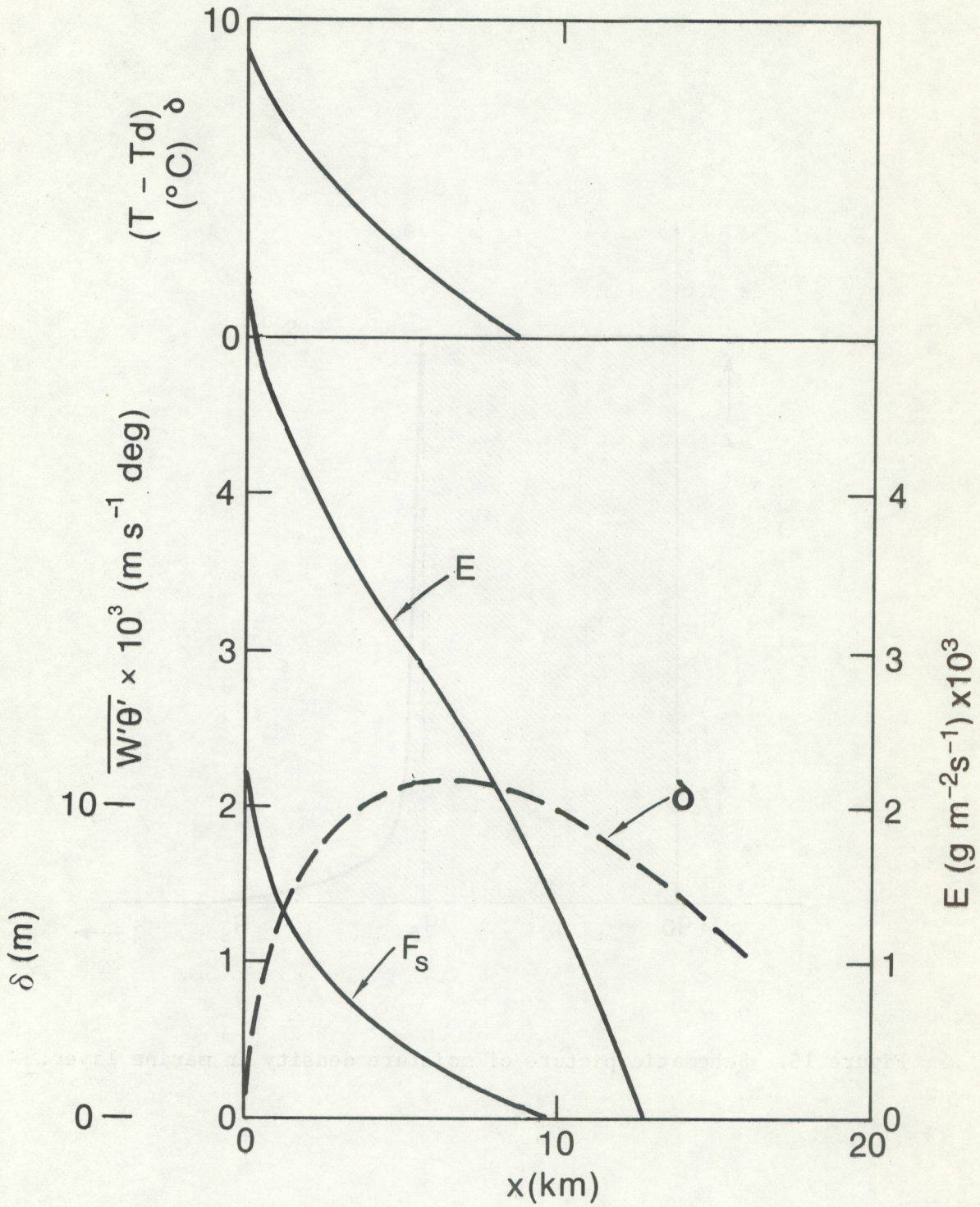

Figure 15. Same as Fig. 13 except F_A = 0.04 deg m s^{-1}.

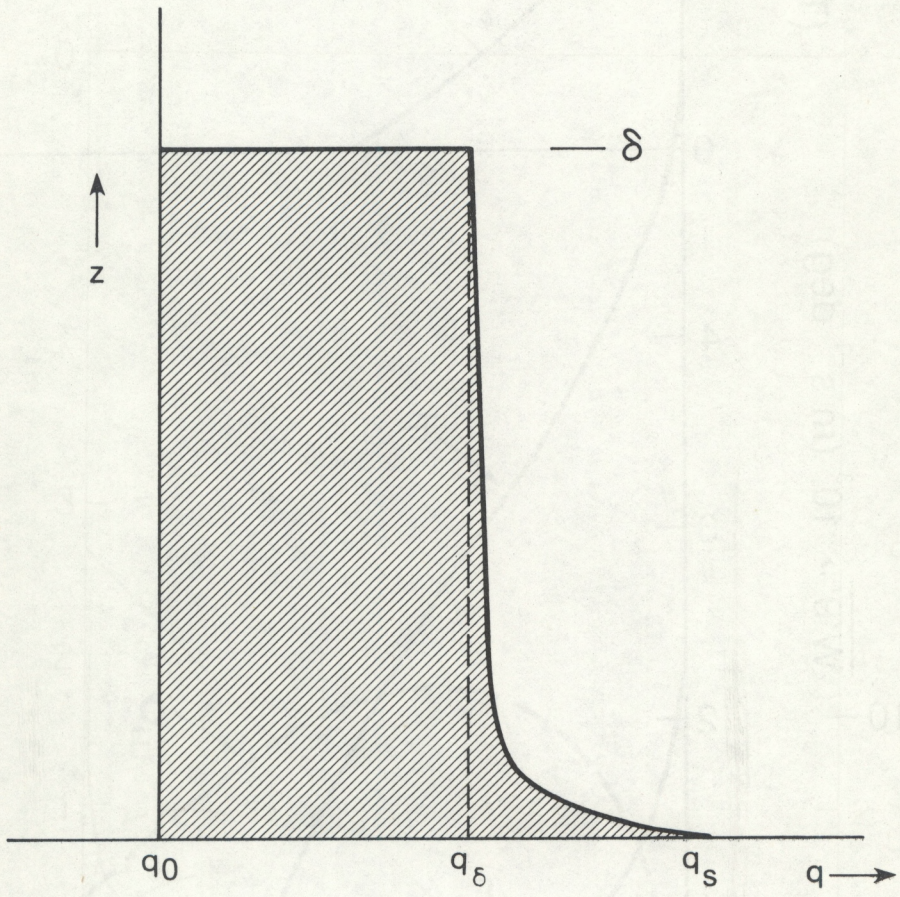

Figure 16. Schematic picture of moisture density in marine layer.

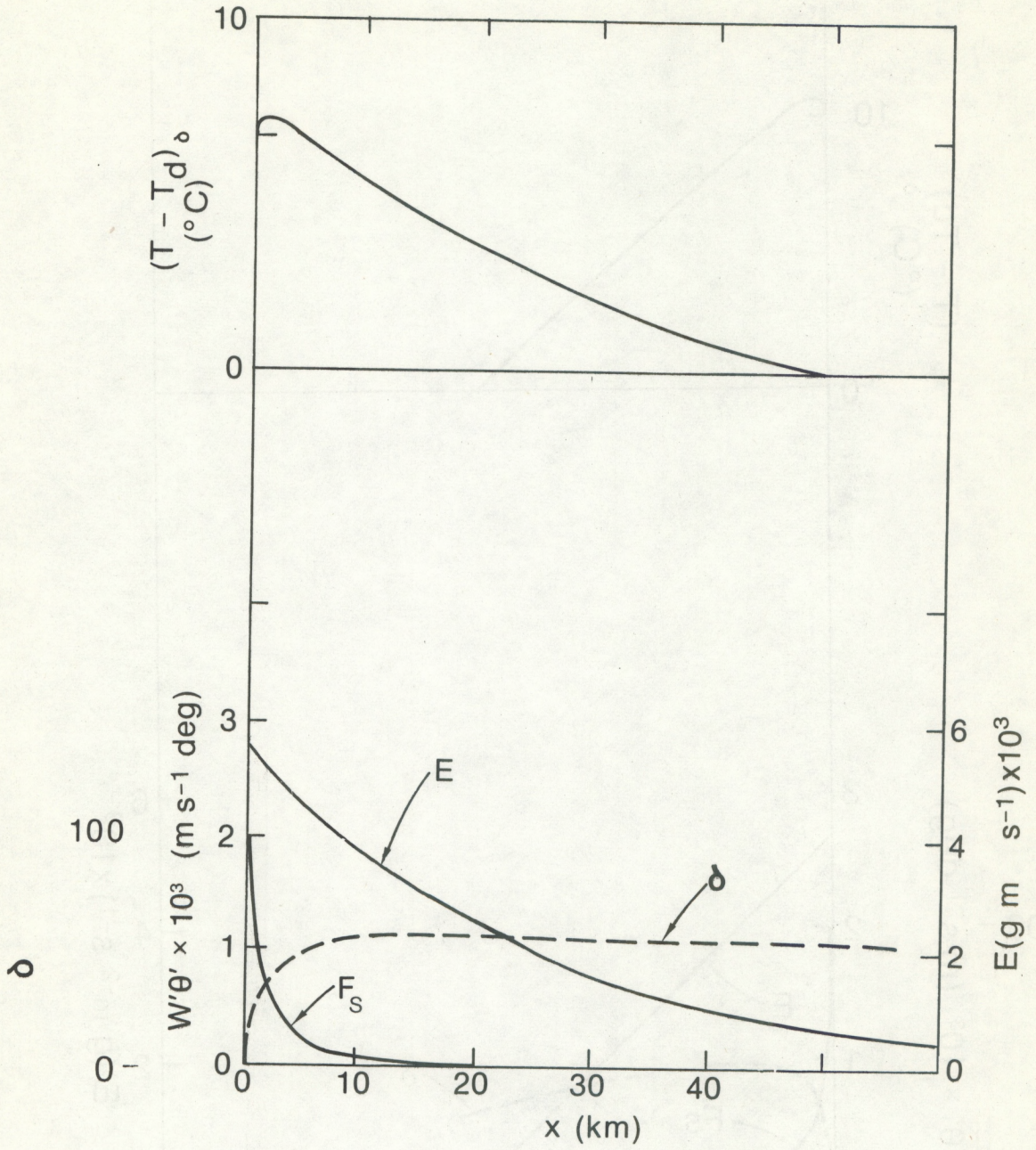

Figure 17. Same condition as in Fig. 13 except C_d = 0.038 and h_o = 300 m.

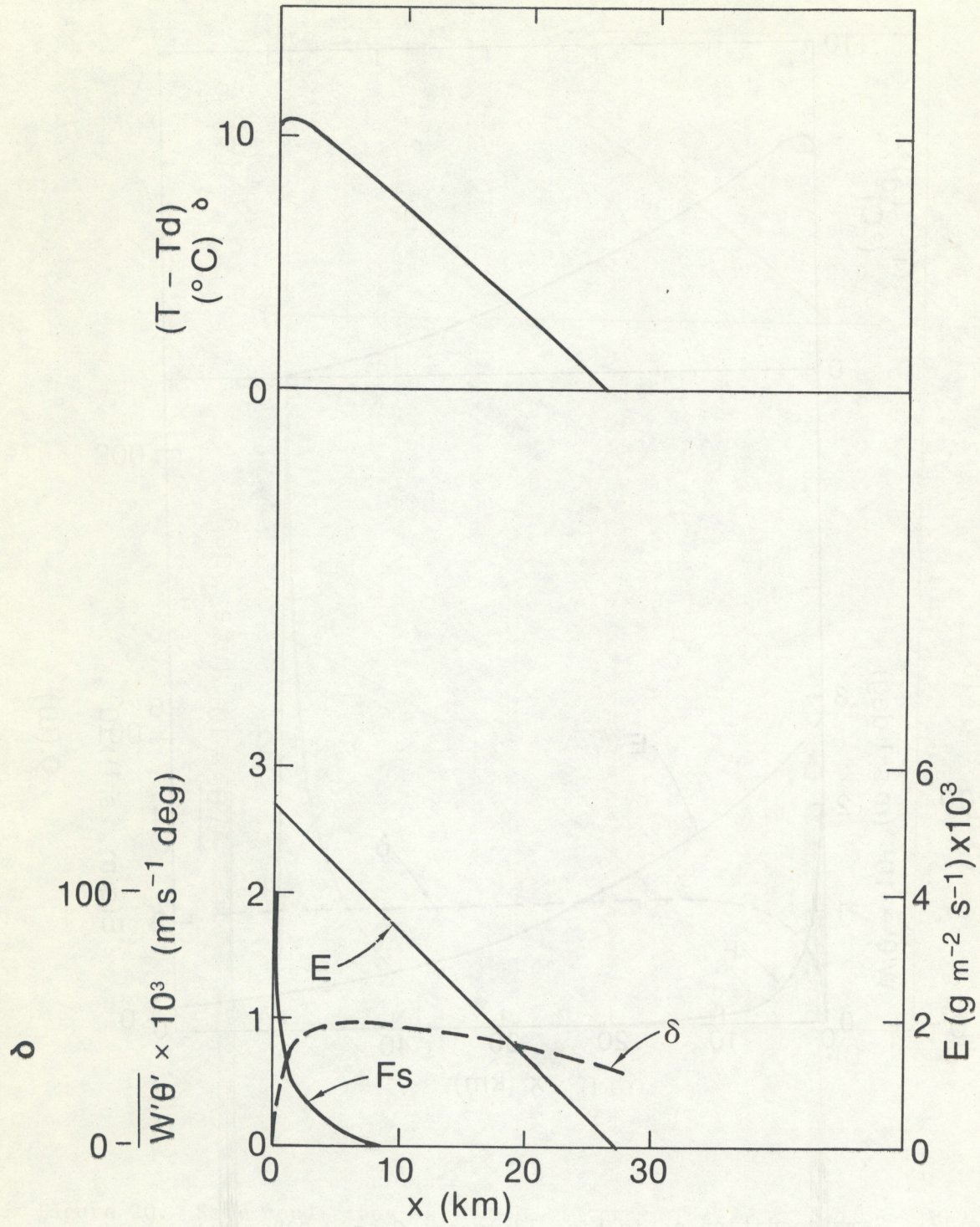

Figure 18. Same condition as in Fig. 15 except C_d = 0.038 and h_o = 300 m.

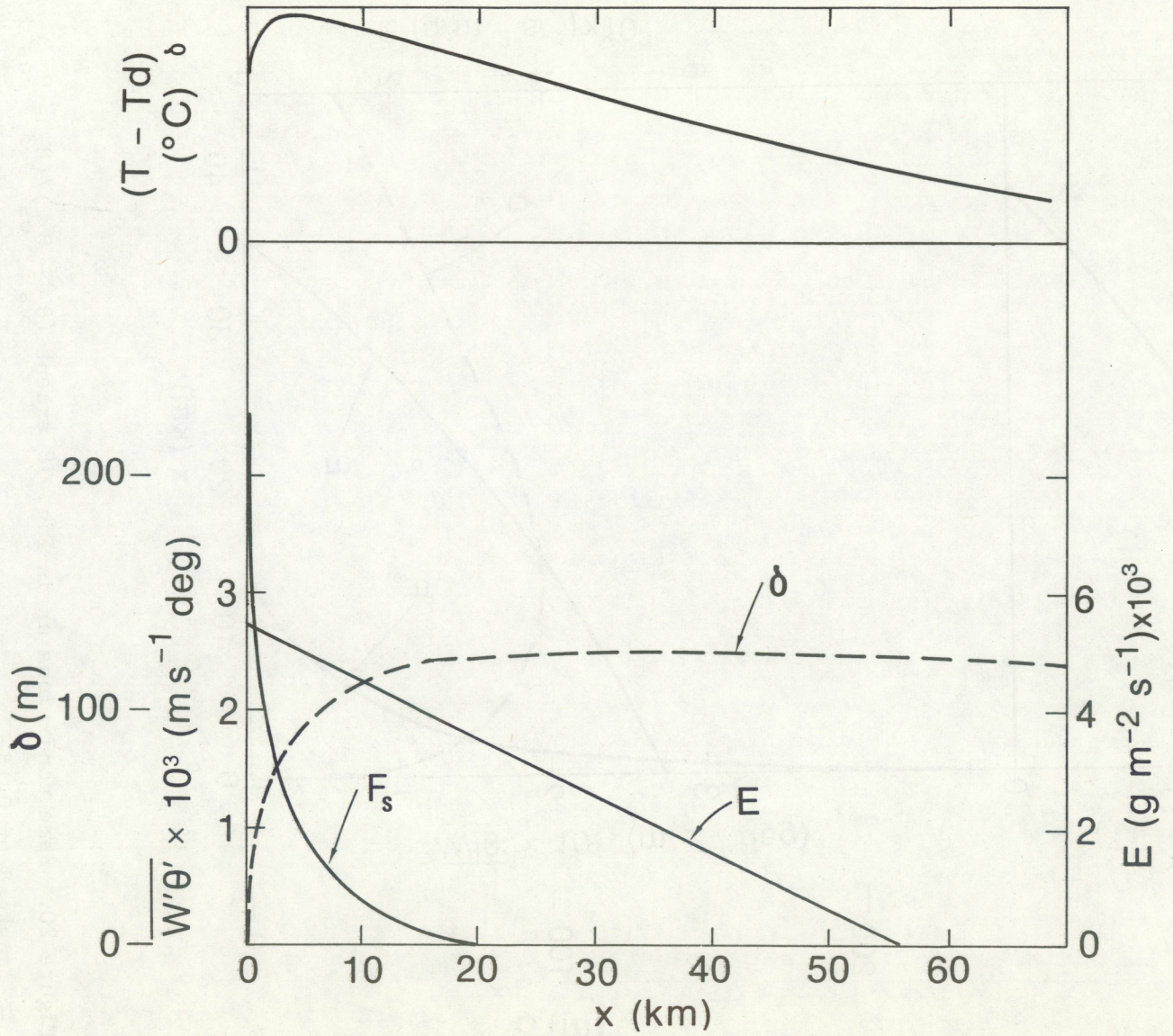

Figure 19. Same conditions as in Fig. 17 except $(\theta_s - \theta_{os})/ (\theta_3 - \theta_{os}) = 0.28$ instead of 0.15.

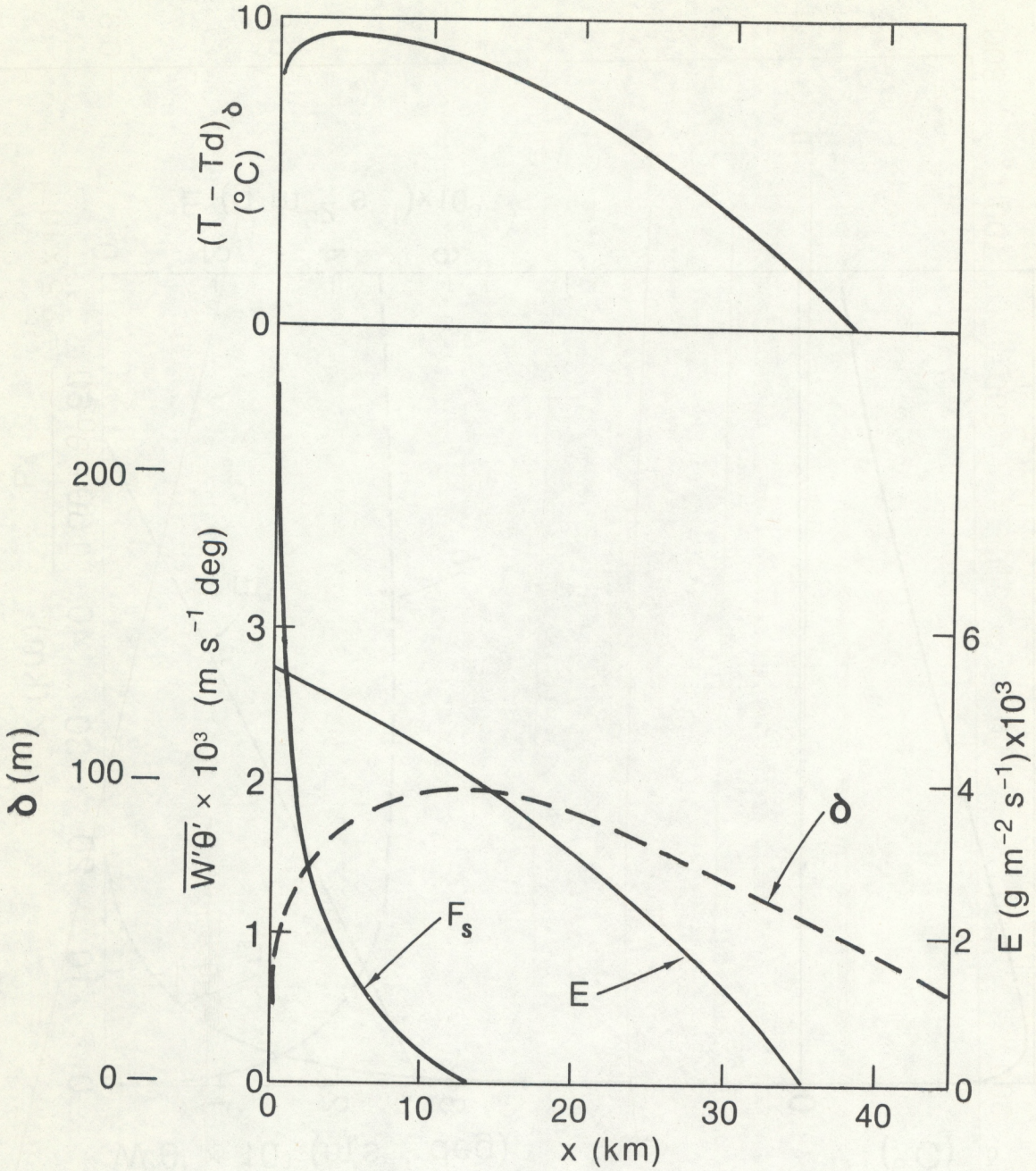

Figure 20. Same conditions as in Fig. 18 except $(\theta_s - \theta_{os})/(\theta_3 - \theta_{os}) = 0.28$ instead of 0.15.

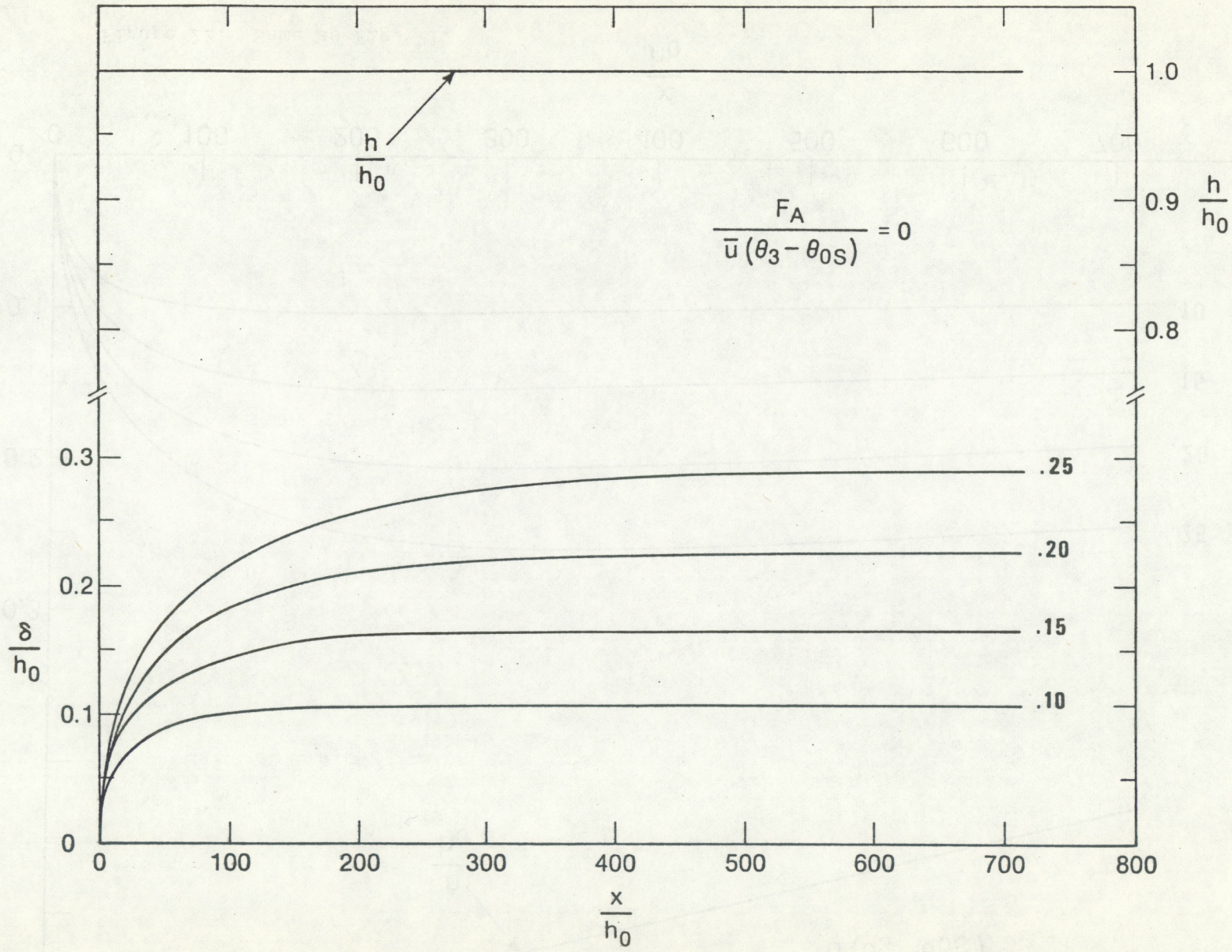

Figure 21. Graphical solution for refractive index gradient at height δ, for various conditions of initial scale height, initial refractive index profile, water temperature and wind assuming $C_d = .0038$. The downward heat flux and/or subsidence is expressed in the parameter $F_A/\bar{u}\ (\theta_3 - \theta_{os})$. Graphs are non-dimensionalized to the scale height of potential temperature in the unmodified air.

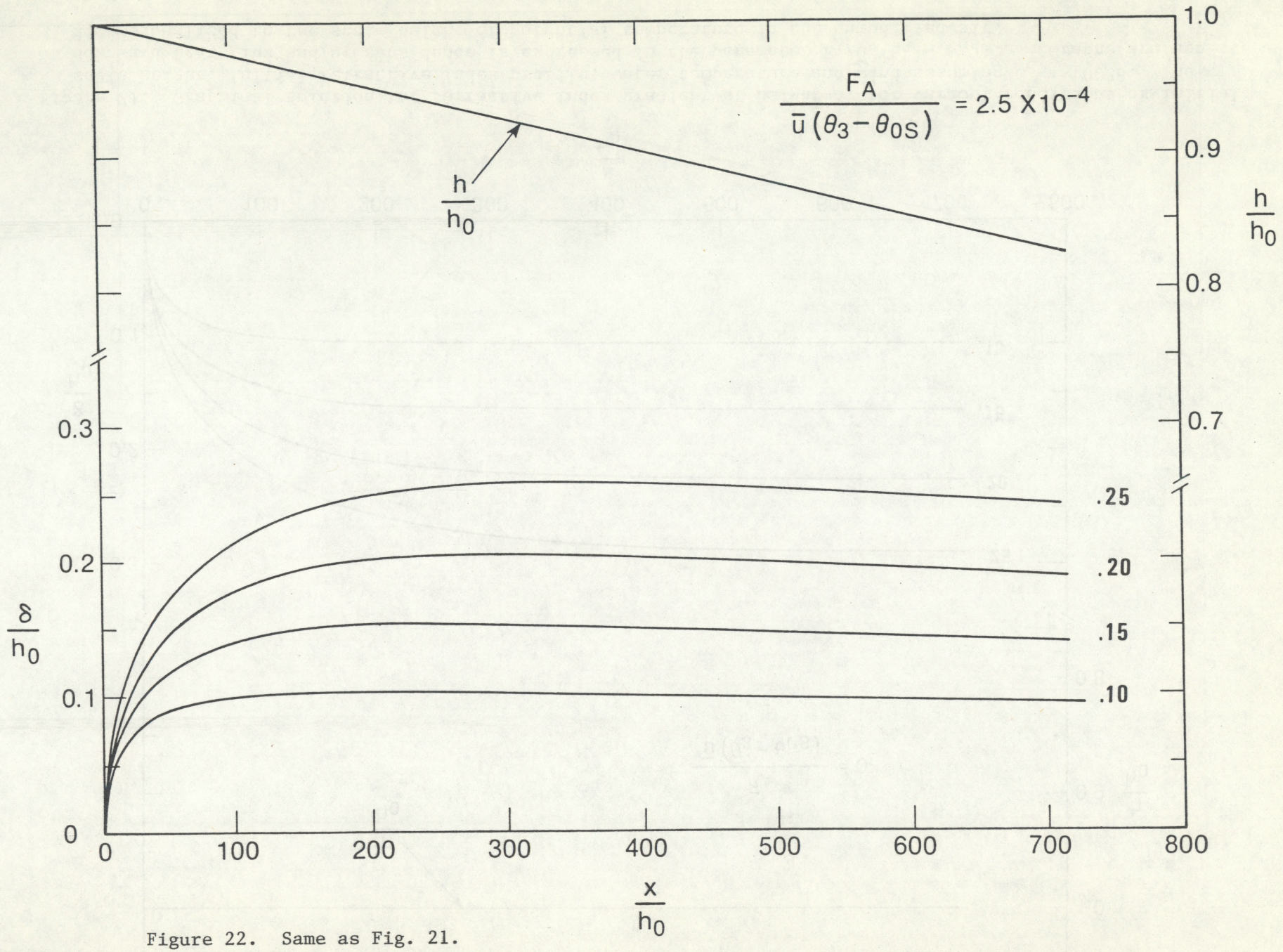

Figure 22. Same as Fig. 21.

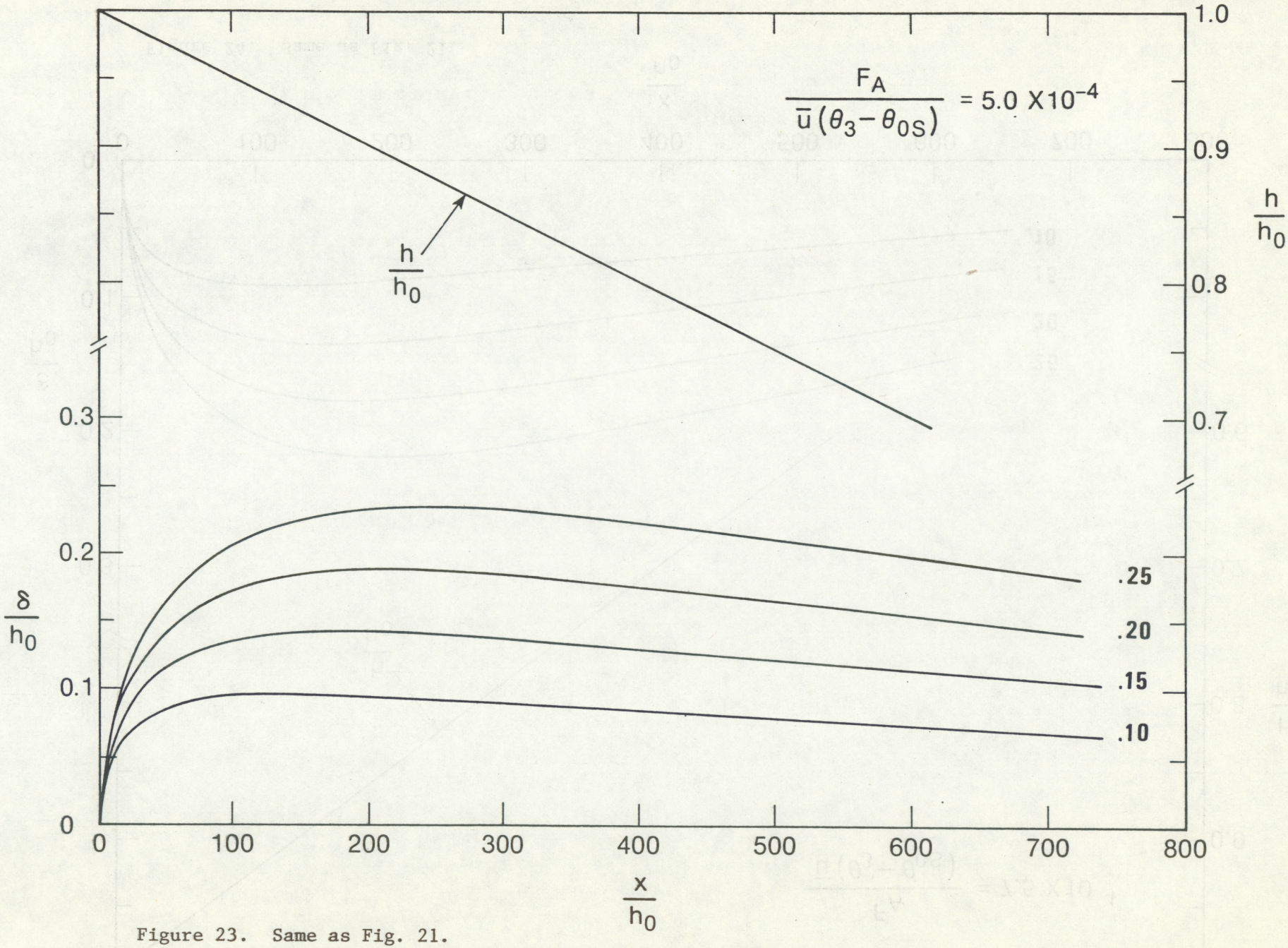

Figure 23. Same as Fig. 21.

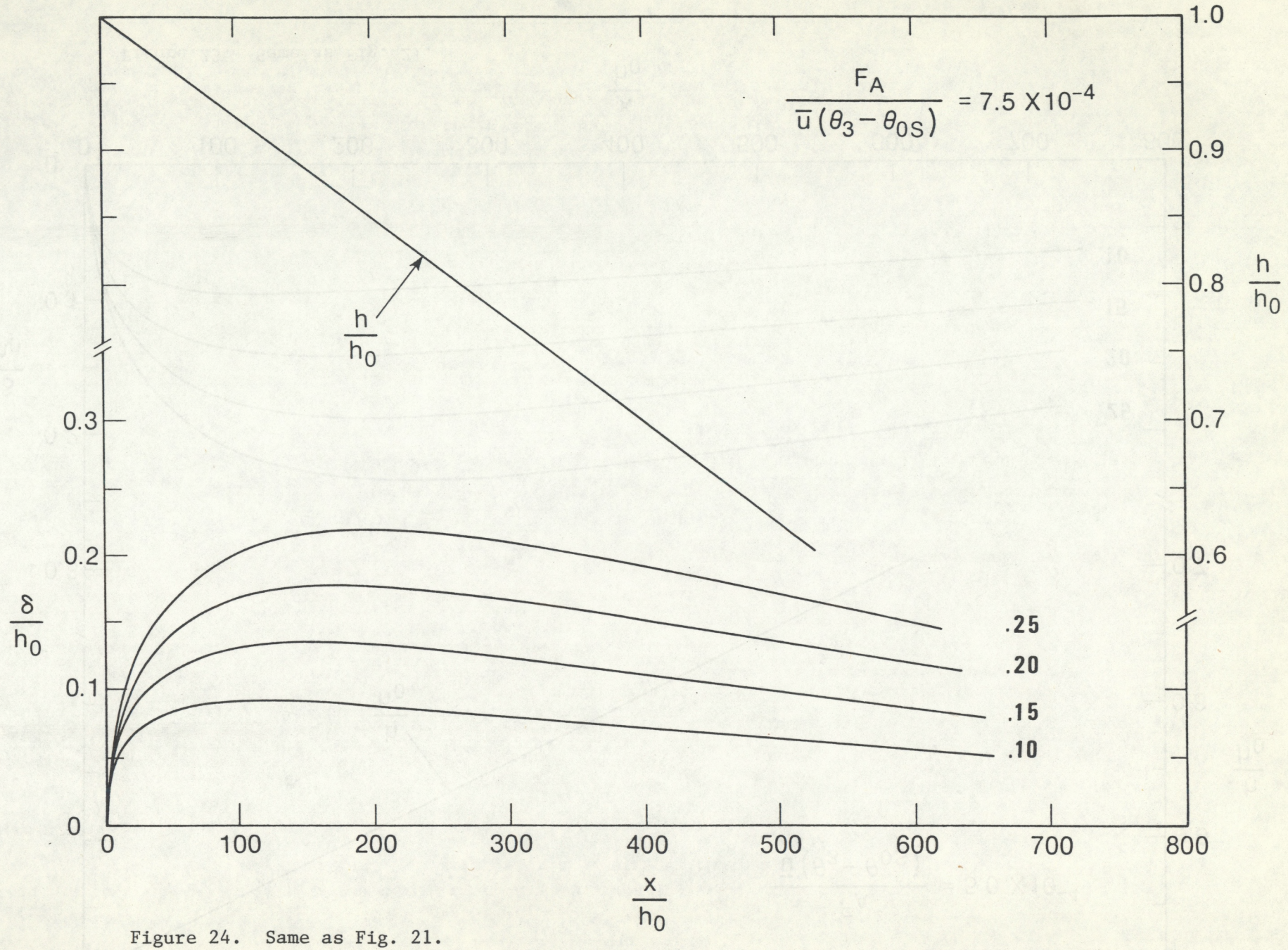

Figure 24. Same as Fig. 21.

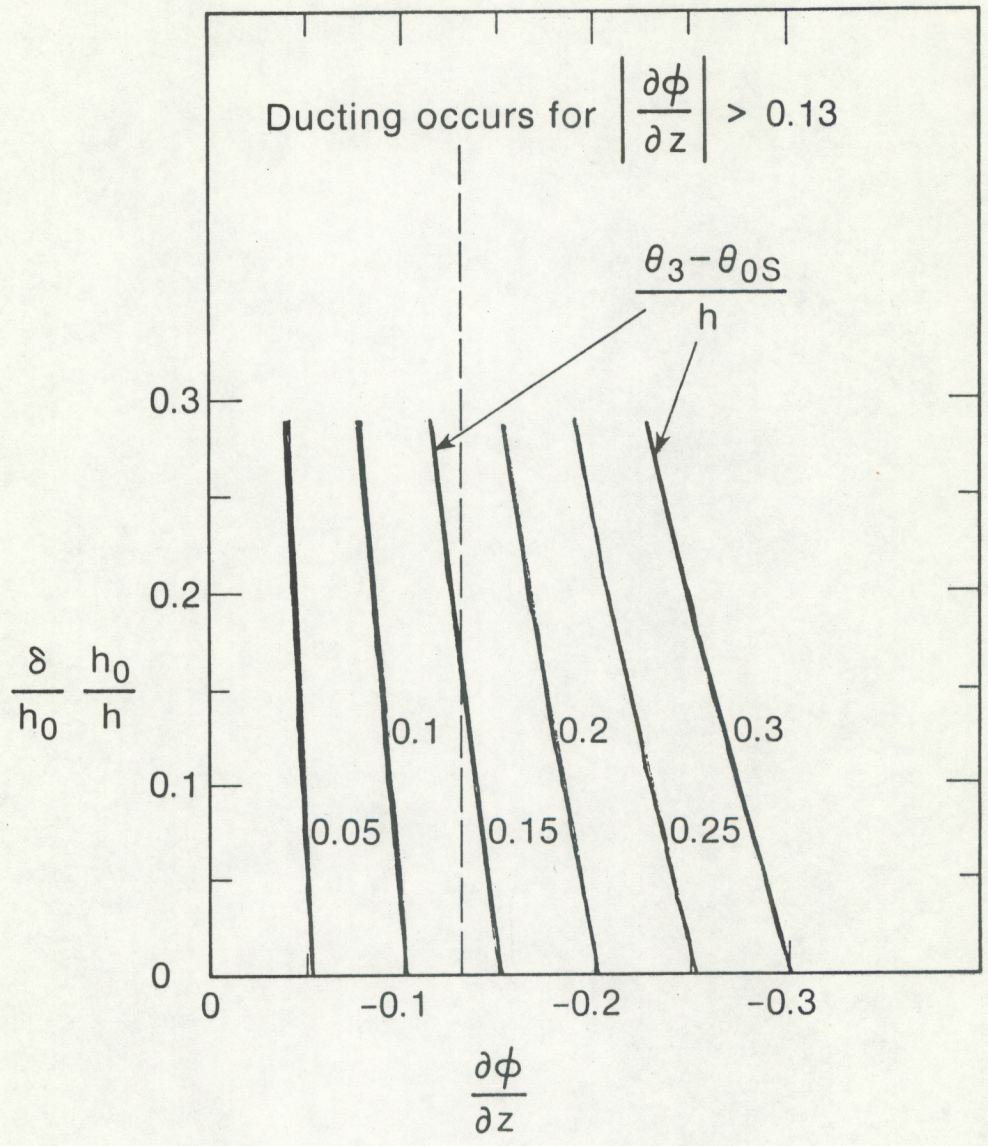

Figure 25. Maximum gradient of potential refractive index at height δ/h. For a known distance x, initial scale height h_o, and initial refractive index height gradient $(\theta_3 - \theta_{os})$, figures 21, 22, 23 and 24 yield $\delta/h \equiv (\delta/h_o)(h_o/h)$ and $(\theta_3 - \theta_{os})/h$ from which $\partial\phi/\partial z$ can be computed. This development assumes the scale heights of potential temperature and potential refractive index are the same.